NTNU
Norwegian University of
Science and Technology

Novel Low Cost Solar Thermal Energy Concepts for Developing Countries

Håkon Jarand Dugstad Johnsen

Master of Science in Mechanical Engineering
Submission date: June 2017
Supervisor: Jan Torgersen, MTP
Co-supervisor: Ole Jørgen Nydal, EPT

Norwegian University of Science and Technology
Department of Mechanical and Industrial Engineering

Summary

Small scale solar thermal energy devices such as solar cookers are promising solutions for remote areas where other energy sources are limited, for instance in developing countries. These devices can be used directly for cooking or for warming water. A successful application of these devices in developing countries requires them to be affordable, robust and easy to use. The use of traditional concentrator based solar cookers is complicated by the need to accurately rotate the large parabolic mirror for solar tracking. In this thesis, a workaround is demonstrated. Via beam-steering lens arrays, sunlight can be tracked with a simulated $\approx$70% efficiency across ±40° tracking range, using millimeter-scale lateral translation and introducing less than $\pm 2^\circ$ divergence to the beam. This eliminates the need to rotate the mirror, facilitating the design of a simpler cooker. Full-day cooking can be achieved by manually reorienting the cooker 1-2 times a day in the general direction of the sun. Accurate automated tracking is performed by small low-cost actuators, and additional features such as adjustable power level can also be implemented.

The optical system was simulated and optimized using Zemax OpticStudio, and a functional 1:15 scale prototype has been constructed. The prototype demonstrates a promising total system efficiency of $\approx$20%, which is expected to rise to 50%-60% with improved manufacturing of the lens array and reflector. The lens array is assumed to be compatible with injection molding, enabling low-cost high-volume production.

By enabling low-cost automatic tracking, this technology may facilitate inexpensive, maintainable and user-friendly solar cooking, fostering its increased adoption across the world. The beam-steering lens array represents developments that are applicable to the wider field of solar energy, with applications such as tracking for concentrator photovoltaic systems and solar lighting systems. A separate journal article has therefore been drafted documenting the development and performance of this technology.

Oppsummering

Småskala termisk solenergi representerer lovende teknologi, spesielt for områder der tilgang på energi er begrenset, slik som i utviklingsland. Termisk solenergi kan brukes direkte til bruksområder som matlaging eller oppvarming av vann. For å kunne anvendes i utviklingsland, må et produkt som anvender termisk solenergi være billig, robust og enkelt i bruk. I tradisjonelle konsentrator-baserte solovner må man stadig rotere det store konsentrator-speilet slik at det alltid er rettet nøyaktig mot solen. Dette fører til dårlig brukervennlighet og/eller kompliserte mekniske systemer. I denne oppgaven presenters det derfor en alternativ løsning. Ved hjelp av beam-steering lens arrays (linsematriser som kan styre en lysstråle) kan sollys følges med en simulert $\approx 70\%$ effektivet over en $\pm 40^\circ$ sporingsområde, ved hjelp av bevegelser på millimeterskala. Systemet introduserer samtidig mindre enn $\pm 2^\circ$ simulert divergens til solstrålene.

Denne løsningen eliminerer behovet for å rotere et stort konsentrerende speil, og legger dermed til rette for design av en enklere konsentrerende solovn. Matlaging gjennom en hel dag kan oppnås ved å manuelt flytte solovnen 1-2 ganger om dagen slik at den peker i solens omtrentlige retning. Nøyaktig sporing gjøres deretter av små, billige aktuatorer. I tillegg tillater teknologien implementasjon av ekstra funksjonalitet som for eksempel regulerbar kokevarme.

Det optiske systemet ble simulert og optimalisert ved hjelp av Zemax OpticStudio, og en fungerende prototype med omtrentlig 1:15 skala ble konstruert. Denne prototypen demonstrer en omtrentlig system-effektivitet på 20%, som forventes å øke til $50\% - 60\%$ med forbedrede produksjonsteknikker. Linematrisene er kompatible med prosesser som injeksjonsstøping, og kan derfor produseres billig i store volum.

Ved å muliggjøre billig automatisk sporing av sollys, kan denne teknologien legge til rette for billig, robust og brukervennlig sol-matlaging, og dermed fremme økt bruk av solovner. Beam-steering lens array er teknologi som er anvendbar også for andre solenergibruksområder som concentrator photovoltaics (CPV) og systemer for solbelysning. Et separat utkast til en tidsskriftartikkel som dokumenterer denne teknologien har derfor også blitt utarbeidet.

Preface and acknowledgments

The motivation for this works stems from my experience from spending 6 months in Northern Uganda through an FK Norway exchange program in 2011-2012. Through conversations with my host family and other friends in the area, I learned about the extensive use of charcoal and wood for cooking purposes, and how deforestation and unpredictable fuel prices were large challenges. During my stay, I experimented with solar cooking and solar water heating, and created several basic solar cookers based on blueprints that were freely available online. When the opportunity arouse to freely define a master's thesis, this was therefore a natural choice. I am forever grateful to my host family, Michael and Immaculate Eluku for hosting me and giving me this valuable experience.

I want to thank my supervisor, Associate Professor Jan Torgersen for believing in me and allowing me to pursue this project despite its uncertain and ambitious nature. I also want to thank my co-supervisor Professor Ole Jørgen Nydal who leads solar cooking research at NTNU for encouraging me to pursue solar cooking and for supervising this thesis despite being on a sabbatical leave. The work would also not have been possible without the support of Professor Astrid Aksnes, who helped me get access to the required software. I also want to thank Børge Holen for his work and assistance on production of the prototypes.

Thank you to my best friend Marie Bjørnevik for always coming up with good ideas and suggested solutions to problems, and thank you to Johannes Lindstad for the safety glasses you gave me.

Finally, I want to thank my family for always being supportive and encouraging.

Contents

Chapter 1

Introduction

1.1 Background

Solar energy is becoming an increasingly important energy source, with solar energy installations growing at increasing rates worldwide [1]. Solar energy can provide low cost, off-grid energy solutions and can be especially useful in developing countries where less developed grid infrastructure is available for energy transport. For thermal applications, significantly higher energy efficiency can be achieved by using direct solar thermal energy instead of PV-elements. This leads to smaller collector sizes and lower price for a given amount of power, and is the focus of the present thesis.

1.2 Problem description

Small scale solar thermal energy devices are promising solution for areas where other energy sources are limited, such as in developing countries. These devices can be used directly, for cooking or for warming water. A successful application of these devices in developing countries requires them to be affordable, robust and easy to use. NTNU has developed a concentrator design with simple geometric elements readily available in developing countries. However, their operation is complicated requiring large structures and compensation of wind loads and complex tracking algorithms. Inspired from research in concentrated photovoltaics, the master student will design a light harvesting solution that allows collecting solar energy by lateral translation of a focusing element. After the simulation and evaluation of test concepts, the student will utilize additive manufacturing to prototype a test device that will be evaluated on its tracking capabilities. Optionally, the student will also develop a control algorithm for solar tracking to obtain a fully functional prototype.

1.3 Choice of target application

In accordance with the problem description, the goal of this thesis is to use principles from recent CPV research to design a new solution for small scale solar thermal energy with focus on developing countries. In order to limit the scope of the thesis, a more narrow target must be defined.

Small scale solar thermal energy has several applications, among others:

- Water heating
- Cooking
- Small scale industrial processes

As shown in Table 1.1, the power and concentration requirements are different for the different applications. For water heating, the power requirements are relatively low since the water heater can spread the heating over the whole day. The target temperatures are not very high, which means that good performance is achievable with low concentration and modest amounts of insulation.

Solar cooking has higher power needs, since all the required energy for cooking should be provided over the short period of time when the user is using the device. The target temperatures are also higher, leading to higher requirements for concentration.

The requirements for small scale industrial processes depends on the specific process, but might be much higher.

	Water heating	Cooking	Small scale industrial processes
Concentration requirements	Low (1x-10x)	Medium (2x-200x)	High (>100x)
Power requirements	Medium (>200W)	Medium (>500W)	High (>2kW)

Table 1.1: Quick comparison of approximate requirements for different small scale solar thermal energy applications.

Based on this assessment, the application of solar cooking has been selected. This application requires solar tracking and modest concentration, without requiring very high precision and high concentration. In order to limit the scope of the project, no heat storage or heat transportation has been considered in the concept development. Future developments could include such concepts.

1.4 Methodology

The scope of this project spans across a wide number of topics including optics, simulation, manufacturing, electronics, control systems and measurement systems. In order to ensure

consistent progress without spending too much time on each sub-problem, a timeline was sketched at the beginning of the project. The timeline included 5 main categories of work, each of which would receive 1 month out of the 5 month total project period:

- Literature search
- Identifying possible concepts and choosing a concept for further development
- Simulate and optimize concept using Zemax OpticsStudio
- Create prototype
- Finalize thesis

Despite the large uncertainties at the start of the project, it has been possible to follow this general outline. The two most notable changes from the original plan has been that optics simulation in Zemax and real-life prototyping has been utilized throughout the whole project and not only in their designated time periods. Creating the extra prototypes has been a motivating factor throughout, and has provided invaluable experience with the development and production of optical systems. The combination of simulation and prototyping has provided hands-on experience for understanding geometrical optics, in which the author did not have any advanced background before the start of this project.

In retrospect, not enough time was allocated to setting up a test protocol and performing thorough testing of the final prototype, which increased the workload towards the end of the project.

1.4.1 Literature search

This thesis is not a continuation of earlier project work, so all search for relevant literature was performed at the start of the period. Google Scholar [2] and Open [3] was used to identify previous NTNU research on solar cooking and solar thermal energy. Different search terms were used, both search terms related to solar cooking/solar energy and directly searching for the names of students and supervisors. 37 publications were identified and added to a Zotero database.

Recent concentrator photovoltaics (CPV) research was identified using Google Scholar [2]. A number of seach terms were used, including the following:

- Solar concentrator
- Solar tracking
- CPV
- Concentrator photovoltaics
- micro planar tracking
- beem steering
- lateral translation solar concentrator

- planar ”solar concentrator”

A total of 92 relevant CPV research publications were indentified and added to a Zotero database.

1.5 Thesis structure

During the development of the solar cooking concept, a new technique for solar tracking through beam-steering has been developed and demonstrated. A journal article has been drafted, which documents the development of this technology and its applications to the wider field of solar energy. The journal article will be submitted for publication after some final adjustments. This thesis therefore consists of two main parts:

- The present thesis, which documents the broader scope of work that has been done during this project, and considers the applicability of the new solar tracking technique for the specific application of solar cooking.
- The draft of the journal article for solar beam-steering, included as Appendix A of this thesis.

In addition, an abstract has been written and submitted for presenting the work at the 2018 CONSOLFOOD Conference [4] in Universidade do Algarve, Portugal. This is included as Appendix B.

1.6 Introduction to solar cooking

A large number of people depend on biomass for cooking purposes, using an average of 0.5-1kg dry biomass per person per day [5, p. 370]. The need to reduce this consumption and find other energy sources for cooking is increasing, due to increasing deforestation and desertification [5, p. 371]. Solar energy is an alternative energy source, and it can be used directly for cooking. Different solar cooking designs have been around for a long time, and organizations like Solar Cookers International [6] are distributing solar cookers worldwide. According to Solar Cookers International, 3.1 million solar cookers have been distributed worldwide by different organizations since 1990 [7].

Solar cookers are used both at the level of individual consumers, and at larger institutions. For individual consumers, solar cooker designs have traditionally been divided into three broad categories [8]:

- Solar panel cooker
- Solar box cooker
- Solar parabolic cooker

In addition, solar cooker designs have broadly been divided into direct and indirect cookers depending on whether a heat transfer medium is used or not [9].

Despite the large international distribution of solar cookers, solar cooking adoption is still relatively low [10]. In an article by Pia Otte, she explains this by developing a list

of 6 categories of factors that influence the adoption of solar cooking: economic, social, cultural, environmental, political and technical factors [10]. For successful adaptation of solar cooking, all of these factors must be considered. The focus of this thesis is to develop technology that support the 6th category: technical factors, such as level of performance and ease of use. Combined with a distribution program that controls the other factors, it is hoped that this can contribute to higher adaptation of solar cookers.

One important cultural factor identified by Otte is that a solar cooker is most likely to be adopted if it corresponds to traditional local cooking habits [10]. Although cooking habits vary greatly across and within different countries, one common factor for most traditional cooking habits is the use of high-temperature heat source usually based on combustion. Cooking with low temperature allows the use of low power and low concentration factors, such as in a solar panel cooker and a solar box cooker, but this requires a significant alteration of cooking habits. This thesis therefore focuses on solar cooking using concentrated solar energy that can provide high temperatures in order to be more compatible with traditional cooking habits.

1.7 Recent developments in Concentrator Photovoltaics

In recent years, there has been an increasing amount of research on Concentrator Photovoltaics (CPV), especially on CPV modules with integrated tracking [11] and low thickness [12, 13].

Research on CPV shares a number of objectives with solar cooking, as indicated in Table 1.2. Therefore, the literature on CPV research has been reviewed, in order to identify concepts that could lead to a solar cooker with improved performance.

Objective	CPV	Solar cooking
Flat concentrator	Yes	Yes
Low cost	Yes	Yes
Integrated solar tracking	Yes	Yes
Very high concentration	Yes	No, modest concentration is enough
One single receiver	No, many small PV modules can be used	Yes
Separation between optics and receiver	No	Yes, optics must be protected from the heat of the receiver

Table 1.2: Comparisons of objectives between CPV and solar cooking

1.7.1 Brief overview of recent CPV research

The field of Concentrated Photovoltacis (CPV) has been developed in order to utilize the high efficiency of expensive multi-junction solar cells, at a lower cost by concentrating the solar energy. Recent developments in the field have focused on increased flatness of optical systems, and on eliminating bulky external tracking structures [11].

Lens array with planar waveguide In 2010, Karp et al. suggested the use of a microlens array coupled to a planar waveguide as a cheap, mass producible way to eliminate bulky mirrors and lenses from CPV systems [12]. A number of people have suggested ways to improve the concentration and optical efficiency of this design [13, 14, 15]. Hallas et al. integrated tracking into Karp's design by laterally moving the waveguide in order to follow the focal spots from the microlens array and achieved good efficiency for a $\pm 10°$ tracking range [16]. Zagello et al. demonstrated automated tracking for a Karp-like design at a range of $\pm 23°$ by using a phase-change material to connect the coupling features at the location of the focal point.

Tracking of solar cell array under lens array Kotsidas et al. examined a design in which tracking is implemented by translating a solar cell array under a stationary lens array [17]. Duerr et al. simplified this system by requiring that the solar cell only moves laterally, and added a second array of laterally translating optics in order to maintain a flat focal plane [18].

Tracking of solar cell array in a folded optical path In 2015, Price et al. suggested the use of an array of a catadioptric optical system, directly illuminating a translatable solar cell array that is sandwiched between the lens and the reflector [19]. This optical setup eliminates the Petzwal curvature and thus achieves 200x concentration over a $\pm 60°$ tracking range [19]. Grede et al. later optimized the optical surfaces in this setup, and achieved $>$1000x concentration over a $\pm 70°$ tracking range [20].

Beam-steering Other CPV research has investigated the possibility of using beam-steering in front of traditional concentrating optics, in order to eliminate external tracking. Some concepts that have been investigated are:

- Electrowetting to change the angle of the interface between two liquids with different refractive indices [21]
- Microfluidic beam-steering arrays [22]
- Rotating prism arrays [23]
- Translating lens arrays [24]
- Using liquid crystals controlled by electric fields [25]
- Rotating off-axis fresnel lenses[26]

Chapter 2

Developing a new solar cooking concept

2.1 Requirements

2.1.1 Possibilities for local production

Many existing solar cooking designs are cheap and low cost, designed to be easily constructed from equipment that is readily available in developing countries, such as cardboard, parabolic antenna dishes, aluminum foil, and so on. This way, the cooker can be built by local craftsmen in developing countries using only local materials. However, these requirements impose a significant limit on what can be achieved. We want to develop a cooker with increased performance and functionality, but this requires custom optical components that must likely be produced using professional industrial processes.

There are still several ways that such a device can be kept affordable in developing countries despite using more advanced production techniques:

- The cookers could be produced using local manufacturing industry in developing countries. For instance, the manufacturing divison of the Mukwano Group in Uganda already produces large quantities of plastic components [27, 28], and has a large distribution network across East Africa.

- There is a market for solar cookers also in industrialized countries. For instance, the SolSource has performed two successful Kickstarter campaigns for solar cookers [29], and their SolSource Solar Grill is sold in the Norwegian retail store Jernia [30]. According to Jon Bøhmer who developed a solar box cooker in Kenya, he was contacted by a large number of interested potential customers from the US [31]. Customers in industrialized nations are likely willing to pay a higher pricer for a cooker, which could help offset the tooling investment costs and allow selling the cooker at a reduced cost in developing countries.

2.1.2 Features

If a solar cooker is going to be supported through commercial volume production, it must be an attractive product that can compete with other means of cooking. In developing countries, the main selling points would be reduced fuel costs. In industrialized countries, idealistic motivations such as aestetics and an environmentally friendly profile are also believed to be important selling points. In all cases, the cooker must be robust, maintainable and easy to use. Despite being used outdoors, it should be possible to store it indoors when it is not in use, for theft protection and protection against the environment.

Based on these considerations, the following user needs are identified for the target users:

- Easy to use
- Easy to store when it is not being used
- Safe
- Works like any other cooker
- Low-cost
- Durable and maintainable
- Manageable size

The focus in this thesis is on developing new technology and concepts for fulfilling these user needs, but a complete product is not designed. For this reason, a detailed set of requirements is not developed, but some performance guidelines are developed in order to evaluate the ability of a concept:

Performance		Reason
Cooking power	≈1kW	The performance should be comparable to other cooking methods.
Effective concentration ratio	$\geq 50x$	Required to supply 1kW to a $180\mathrm{mm}$ diameter cooking surface.
Automated tracking range	$\geq \pm 40°$	The cooker should be easy to use. The user should not need to think about reorienting the cooker more than once a day.
Cost of parts	$\approx$ 200USD or as low as possible	Very uncertain. Depends on which market is targeted. For industrialized markets, a higher price can be accepted, possibly subsidizing a lower prize in developing markets.

Table 2.1: Performance guidelines for a new solar cooker concept

2.2 Concept development

2.2.1 Concept classification

Common to the CPV research that has been highlighted in Secion 1.7.1 is the use of arrays of small subsystems working in parallel as opposed to one large optical system. The use of parallel subsystems enables more compact optics, and it is not unique to recent CPV research:

- Thin Fresnel lenses with many parallell optical paths are well-established as an alternative to thick lenses or thick parabolic reflectors [32].
- Small camera modules working in parallel are becoming an alternative to large DSLR cameras [33].
- Concentrator designs from the field of nonimaging optics are usually large, but their size has been reduced by using parallel optical subsystems [34, p. 193].

This thesis investigates how the same design philosophy can be used for design of small scale solar cooking concepts. In order to develop a new solar cooking concept based on parallel subsystems, we propose a new classification of concentrated solar energy systems (including thermal and PV systems). We then organize the research presented in Section 1.7.1 within this classification. The classification is based upon some of the sub-problems that must be fulfilled by a concentrated solar energy system, namely:

Tracking: Keeping the system in focus despite the apparent motion of the sun across the sky.

Concentration: Increasing the flux density of the sunlight.

Conversion: Converting the electromagnetic energy to thermal or electrical energy.

We propose that a concentrated solar energy system can be classified depending on which of these sub-problems are solved within the context of the small parallel optical subsystems:

1. Only **tracking**: Known as beam-steering designs [11], the parallel sub-systems perform only tracking. They are placed in front of another system where concentration and conversion occurs as illustrated in Figure 2.1a.
2. **Tracking** and **concentration**: Karp et al. [12] and derived designs [13, 14, 15, 16] track[1] and concentrate the solar energy. A planar light guide is used to transport the energy to the edges of the optical system, where conversion occurs as illustrated in Figure 2.1b.
3. **Tracking**, **concentration** and **conversion**: A number of CPV designs, such as Kotsidas et al. [17], Duerr et al. [18] and Price et al. [19] propose the use of small PV elements in each parallel sub-system as illustrated in Figure 2.1c.

[1]The original Karp-design did not include tracking [12], but this was quickly added in derived designs. For simplicity, it is therefore included as tracking and concentration.

4. **Concentration** and **conversion**: Traditional CPV designs did not include tracking in the parallel sub-systems. Concentration and conversion has typically been done in parallel optical sub-systems, while tracking was implemented by mechanically rotating the entire CPV module [11].

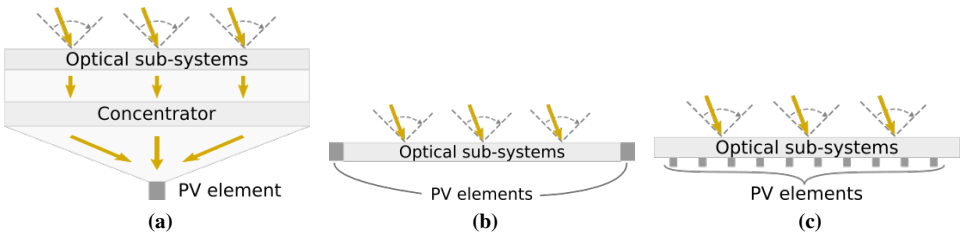

Figure 2.1: Illustration of different categories of recently proposed CPV designs

When developing a concept for solar cooking that uses parallel optical sub-systems, the same choice must be made as to which problems should be solved by the parallel optical sub-systems:

1. Only **tracking**: The parallel optical subsystems perform tracking through beam steering in front of traditional concentrating optics for solar cookers.

2. **Tracking** and **concentration**: By combining tracking and concentration in the parallel sub-systems, very thin concentrating optics can be created. Recent literature has suggested how this can be used for thermal energy by using air gaps to protect the optical system from excessive heat [35]. However, for solar cooking, the highly concentrated solar energy, with a total flux of up to a kilowatt, must be transferred a distance on the order of 1-2 meters. This requires very accurate optics and/or a high-quality light guide in order to limit unwanted local heating and potential thermal runaway at imperfections in the light guide.

3. **Tracking**, **concentration** and **conversion**: Including conversion in the parallel optical sub-systems would involve many small absorbers, and some form of heat transfer to the place where the heat will be used. For thermal systems, this is therefore a very complex solution.

Based on this assessment, a parallel optical sub-system that only implements tracking is selected for this thesis. There might be further benefits to gain from including concentration in the parallell optical sub-systems, but the uncertainties with regards to optical quality and the risk for thermal runaway were deemed too large for this thesis. Therefore, the first alternative of only impelementing tracking in the parallel optical subsystems is selected, and a beam-steering concept is created.

2.2.2 Choosing a beam-steering concept

A large number of different beam-steering concepts have been proposed in the literature, some of which are listed in Section 1.7.1. From this list, beam-steering lens arrays [24] stand out as a system with a number of benefits:

- They lend themselves to high-volume production techniques such as injection molding or hot embossing.
- Development does not require high-tech materials, enabling a fast development phase both for this thesis and for potential commercialization.
- The optics are similar to the optics used in many of the other CPV designs, which means that the other designs can be used as inspiration for design concepts and production techniques.

Some of the other beam-steering designs based on microfluidics [22], electrowetting [21] or liquid crystals [25] indicate improved performance over translating lens arrays, but due to the extra complexity of these systems, they will not be considered for this thesis.

2.2.3 Development of translating beam-steering lens arrays

As described in Section 2.2.2, translating beam-steering lens arrays appear to be a promising solution. However, the existing research does not cover the ways that such a system would be used in a solar cooker:

- A number of publications describe the use of beam-steering lens arrays for steering of laser beams [36, 37, 38]. For these systems, incoming beams are parallel to the optical axis of the system, and emitted at a controlled angle. This is the reverse of what is required for solar energy, where sunlight is received at an angle to the optical axis, and emitted parallel to the optical axis. These beam-steering systems for lasers also have a low tracking half-angle of less than $10°$, which is too low for practical solar cooking.
- Lin et al. has shown promising results with a beam-steering lens array designed using the Simultaneous Multiple Surface (SMS) method that can track incoming light over $\pm 45°$ [24]. However, the performance is only demonstrated for extruded two-dimensional optics, so the system can only track about a single axis. In addition, the aspherical vertical translation required for the wide-angle tracking is difficult to implement kinematically without using separate actuators for all six degrees of freedom.

The concept therefore had to be developed further before it could be used in a solar cooker. This has been a major part of the workload in this thesis, and a journal article reporting the results has been drafted. The draft is included as Appendix A, and will be submitted for publication. In addition, the work is documented in Chapter 3.

2.2.4 Integration of beam-steering lens arrays in a solar cooker

In order to integrate a beam-steering lens array in a solar cooker, it must be combined with conventional concentrating optics. The simplest and most common type of concentrating optics for high-concentration solar cookers is a single parabolic mirror. This is therefore what will be considered for the following thesis. A possible implementation of such a system is illustrated in Figure 2.2, where an off-axis parabolic reflector is used. No heat storage or heat transport is considered for the present thesis.

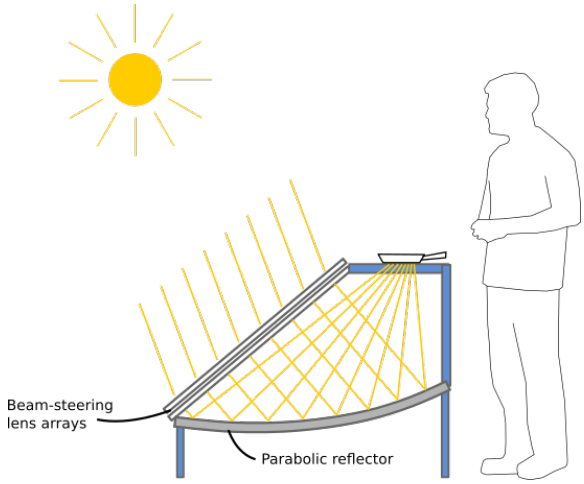

Figure 2.2: Illustration of how a beam-steering lens array can be combined with an off-axis parabolic reflector in a solar cooker concept.

2.2.5 Cooker size

There is a trade-off between cooking power and cooker size. This is illustrated in Figure 2.3 for a solar cooker based on a beam-steering lens array and a design inspired by Figure 2.2. Cooking power of a direct solar cooker without heat storage is low compared to other cooking appliances, unless the solar cooker is very large. One possible remedy is to make the solar cooker collapsible, so that it takes up less space in storage and is easier to carry despite its large dimensions, but this has not been considered in the present thesis.

Based on the size comparison in Figure 2.2, 500W-750W appears to be achievable within a reasonable cooker size, while anything bigger becomes impractical without a good system for quickly collapsing the cooker for storage and transport. Requirements for the beam-steering lens array are therefore developed for a 750W cooker.

2.2.6 Beam-steering lens array requirements

An ideal beam-steering lens array would emit perfectly collimated light. However, due to aberrations and imperfections, it will necessarily introduce some divergence in addition to the $\phi = 0.27°$ divergence half-angle inherent in sunlight [39, p. 49]. After striking the parabolic reflector, the energy will travel unguided until it reaches the cooking surface, so the divergence of the light must be small enough that all the energy will strike within the area of the cooking surface. For the 750W cooker shown in Figure 2.3, the largest unguided distance is from the lowermost corners to the cooking surface, and is approximately $L_{max} \approx \sqrt{(1000\text{mm})^2 + (650\text{mm})^2} \approx 1200\text{mm}$ (using measurements from Figure 2.3). If the cooking surface is assumed to be $\varnothing 180\text{mm}$, the maximum permissible divergence half-angle in order for all the energy to reach the cooking surface is $\phi_{max} = \arctan\left(\frac{90\text{mm}}{1200\text{mm}}\right) = 3.5°$. In order to provide some acceptance for imperfections

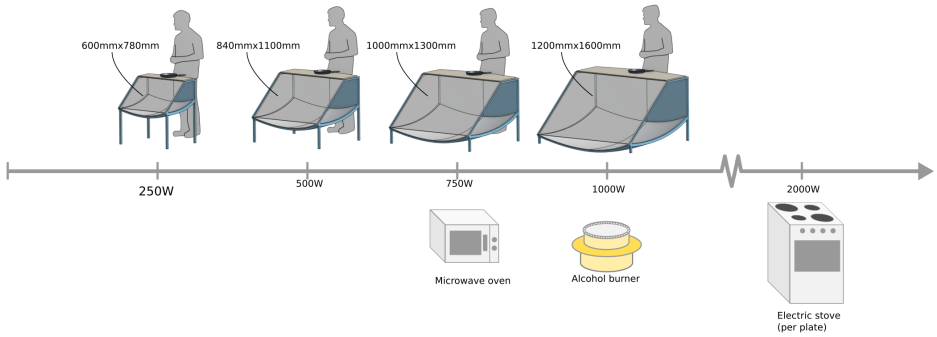

Figure 2.3: Illustration of solar cooker sizes for different power levels, compared to typical maximum power for some other cooking appliances. The sizes assume $900^{\mathrm{W}}/_{\mathrm{m}^2}$ solar insolation and 60% solar cooker efficiency. Cooking power for sources common in developing countries, such as wood and charcoal, depends on a large number of factors, and approximate figures have not been aquired. They are therefore not included in the present figure, but are assumed to be on the order of a kilowatt or more.

in the incoming solar energy, the beam-steering lens arrays have been optimized for an outgoing divergence of less than $2.5°$.

2.2.7 Using a secondary mirror

When developing the requirement of a divergence less than $2.5°$, the normal area of the cooking surface has been used. In reality, rays from the lowermost corners of the off-axis parabolic mirror strike the cooking surface at a high incident angle. With a configuration similar to the sketch shown in Figure 2.2, the highest incident angle on the cooking surface is approximately $60°$, effectively shrinking the projected area of the cooking surface. This leads to a decreased ϕ_{max}:

$$\phi_{max} = \arctan\left(\frac{90\mathrm{mm} \cdot \cos(60°)}{1200\mathrm{mm}}\right) = 2.1° \tag{2.1}$$

This is an inherent problem with parabolic concentrators, leading to decreased maximum concentration factors achievable with a bare parabolic reflector [40, p. 140], but the effect is especially strong due to the short focal length (low f-number) and off-axis nature of the parabolic reflector.

The effect can be mitigated in several ways, as described by Chaves in Introduction to Nonimaging Optics [40, chap. 5]. One simple partial mitigation is to use a flat secondary mirror as illustrated in Figure 2.4. There are some limations to this, however, since the secondary mirror must not shade the sunlight from any other part of the parabolic mirror. For a complete system, a more detailed optical design and optimization of the concentrator must be performed, but in order to limit the scope, this has not been performed in the present project.

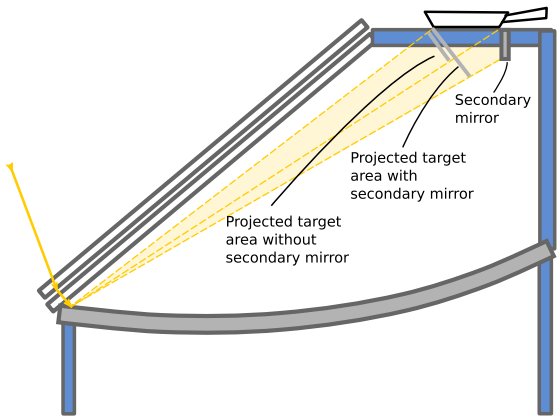

Figure 2.4: Illustration of how the divergence tolerance from the lowermost part of the parabolic mirror can be increased by using a secondary mirror.

Chapter 3

Development of a beam-steering lens array

In order to implement beam-steering using lenses, a pair of lenses are aligned in an afocal configuration: Collimated light enters one lens, and the light is again collimated by the second lens. By translating the lenses so that their optical axis is offset relative to each other, beam-steering is achieved as illustrated in Figure 3.1a. In order to keep the overall dimensions of the system small, small lenslets[1] are arranged in an array, as illustrated by the two neighboring lenslets shown in Figure 3.1a.

Beam-steering lens arrays have previously been proposed for steering of laser beams [36, 37] and also recently for solar energy and steerable LED lighting applications [24]. For laser beam-steering, a beam-steering lens array receives a beam parallel to its optical axis and emits it at an angle. For solar energy applications, the beam-steering lens array must be operated in reverse, receiving a beam at an angle, and emitting it parallel to the optical axis.

A beam-steering lens pair can be Keplarian, using two converging lenses, or it can be Galilean, in which one of the lenses is converging and one of the lenses is diverging [24]. In this work, the best performance was achieved using Keplerian configuration, so that is the focus of the present thesis.

3.1 Beam-steering using thin lenses

Within the limits of the paraxial domain, a Keplerian beam-steering lens array consists of thin converging lenslets separated by their total focal lengths $f_1 + f_2$ as illustrated in Figure 3.1a. Such a system can track incoming sunlight at an angle θ by translating the

[1] Different terminology is used in different publications for similar concepts, including “lens array”, “lenslet array” and “micro lens array”. For simplicity, this thesis adopts the term “lens array” describing the array, and the term “lenslet” for individual lens elements in the array.

last lens array a distance Δx:

$$\Delta x = f_1 \cdot \tan\theta \tag{3.1}$$

In order for all rays to reach the correct lens in the array L_2, the second focal length must be smaller than the first, giving an angular magnification factor M:

$$M = \frac{f_1}{f_2} = 1 + \frac{N}{2}\tan\theta_{max} \tag{3.2}$$

Sunlight has an inherent divergence of $\pm 0.27°$ [39, p. 49]. In order to allow high concentration optics behind the beam-steering lens array, it is desireable that this divergence is increased as little as possible, so the angular magnification of the system should be low. By adding a field lens L_f to the system, as shown in Figure 3.1b, identical focal lengths and an angular magnification of unity can be achieved [36].

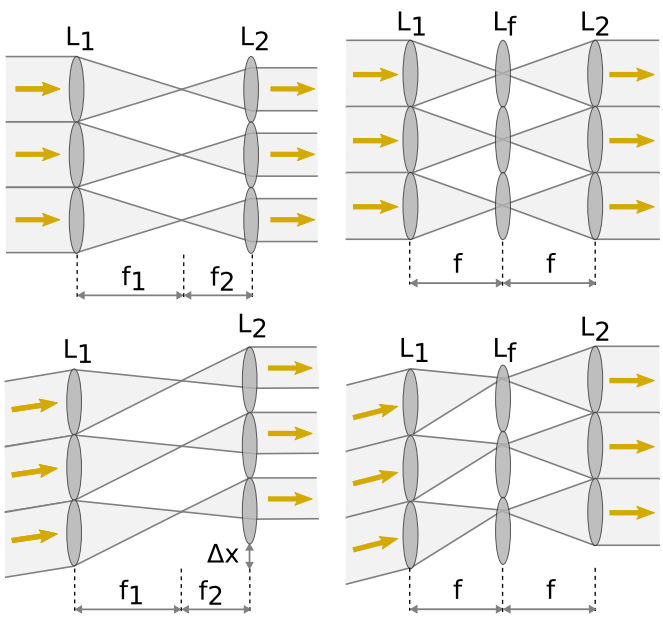

(a) Keplerian beam-steering principle, using back-to-back lenses with different focal lengths.

(b) Keplerian beam-steering principle including field lens and lenses with equal focal lengths.

Figure 3.1

3.2 Challenges to overcome for a practical beam-steering lens array

In order to implement a beam-steering design with high efficiency over a large field of view, some modifications must be done to the basic principles in Figure 3.1a and Figure 3.1b:

- With Fresnel reflection losses of approximately 4% per optical surface[2], it is desirable to avoid the two extra surfaces of the field lens in Figure 3.1b. Therefore, lens array L_1 is instead made thicker so that its second surface partially fulfills the purpose of a field lens.
- For wide field of view, field curvature becomes significant, and purely planar tracking is not sufficient.
- The wide field of view and wide lenses operate outside the paraxial domain, and large aberrations are introduced. In traditional lens design, aberrations are reduced by introducing additional optical surfaces and using apertures that are smaller than the system diameter. Due to the close packing in a lens array, no lens can be wider than the system aperture, and for efficiency reasons, additional surfaces can not be added. Aspheric surfaces must therefore be used to compensate for the aberrations.

3.3 Choosing a material

The material requirements for the beam-steering lens array are similar to other optical components that are used for solar energy optics, such as Fresnel lenses, namely:

- High transmission for solar radiation
- Low dispersion
- High durability in an outdoors environment
- Low cost
- Compatible with high-volume production

The two most common materials for such applications are PMMA (monolithic) and PDMS (applied to a glass backing) [41]. PDMS has slightly improved optical properties and improved radiation resistance, but on the other hand it suffers from increased soiling by readily accumulating dust and other particulate matter on the surface [41]. When PDMS is used for Fresnel lenses, the increased soiling can be avoided by only exposing the bare glass to the environment, while sealing the inside of the lens where the PDMS is applied. This is less practical for a beam-steering lens array where both sides of each array is optically active. Due to these challenges, and the overall simplicity of a monolithic array that can be molded in one piece, PMMA is chosen for this development.

[2] In the scope of this project, anti-reflective coatings have not been considered.

If the material is changed in future developments of the concept, the geometry of the lenslets must be re-optimized/re-designed for the new refractive index, but the same overall concept can still be used.

3.4 Modelling in Zemax

Optical design of a system with the desired properties can be done using a number of techniques:

- Analytical methods such as the Simultaneous Multiple Surface method (SMS method) [40, p. 271].
- Analytical and optimization routines that reduce third order aberrations of the system.
- Optimization techniques that directly optimize for the desired qualities in the system.

In order to limit the scope, only direct optimization techniques are used in this project. This optimization is performed using a legacy version of Zemax OpticsStudio (2009 version) running in sequential mode.

A three-dimensional model of the beam-steering lens array was created in Zemax for optimization. The close hexagonal packing of the lenslets in the lens array is simulated by applying a hexagonal aperture to all surfaces. As will be described in Section 3.4.1.2, the system has been analyzed in focal mode in Zemax even though the system is afocal, and performance is evaluated by evaluating the ray distribution on a distant surface.

The optical system consists of the following surfaces, as can also be seen in the Lens Data Editor shown in Figure 3.2:

- Surface 0: Afocal objective, representing the sun.
- Surface 1: Spacer surface.
- Surface 2: Coordinate break surface. Used with the multi-configuration functionality in Zemax to choose incoming solar angle[3].
- Surface 3: First surface of first lenslet. Modelled as an asphere with even polinomial terms and hexagonal aperture.
- Surface 4: Second surface of first lenslet. Thickness of this surface is the separation between the lens arrays in their $0°$ configuration.
- Surface 5: Coordinate break surface. Used in combination with multi-configuration functionality in Zemax to implement translation of the lenslets for tracking.
- Surface 6: First surface of second lenslet.

[3]Zemax has built-in support for multiple fields, but this is usually used for optimizing a single lens over a larger field of view. In order to clearly separate which field applies to which configuration, a coordinate break is therefore used instead.

- Surface 7: Second surface of second lenslet.
- Surface 8: Spacer surface. Used as last visible surface when displaying 3D layout and similar views.
- Surface 9: Image surface. Placed at a large distance in order to be able to use focal analysis methods even though the system is afocal, as described in Section 3.4.1.2.

Lens Data Editor: Config 4/4

Edit Solves View Help

Surf	Type	Comment	Radius		Thickness		Glass	Semi-Diameter		Conic		2nd Order Term		4th Order Term	6th Order Term	8th O
OBJ	Standard		Infinity		Infinity			Infinity		0.000						
1	Standard		Infinity		1.846			3.397		0.000						
2	Coordinat..				0.000		–	0.000				0.000		0.000	40.000	
*	Even Asph..		4.327	V	5.943	V	PMMA	3.164	U	-0.186	V	0.000		4.654E-006	6.310E-009	2.
4*	Even Asph..		-4.869	V	3.655			3.164	P	0.420	V	0.000		-2.523E-004	8.540E-005	1.
5	Coordinat..				-1.122		–	0.000				0.000		3.519	0.000	
6*	Even Asph..		2.163	V	6.165	V	PMMA	3.164	P	-1.034	V	0.000		-0.013	-8.398E-003	1.
7*	Even Asph..		-2.697		9.230			3.164	P	-1.000		0.000		-3.231E-003	5.762E-004	-4.
8	Standard	Display end	Infinity		1500.000			5.538	U	0.000						
IMA	Filter4	Filter	Infinity		–			80.000	U	0.000		80.000	P	0.200		

Figure 3.2: Part of the Lens Data Editor in Zemax showing the configuration that is used for simulating the lens array.

3.4.1 Merit function

Zemax uses the concept of a Merit function to define optimization objectives[4]. Zemax provides functionality for automatically generating a merit function, but this is designed for optical systems whose imaging properties are more important than overall system efficiency. The default merit function therefore optimizes with respect to imaging properties, and prefers a vignetted ray to an abberrated ray. In our case, high efficiency is more important than perfectly aberration-free performance, so the built-in merit function does not fit our purpose.

3.4.1.1 Algorithm for merit function

The overall purpose of the system is to redirect light from one direction to another, with as high efficiency as possible and within some divergence limit ϕ. This can be expressed using the pseudocode in Algorithm 3.1.

The bold section of Algorithm 3.1 is used to gradually accept a ray as it moves from being outside the permissible exit cone of ϕ to being inside. Otherwise, there would be abrupt changes to the merit function when a ray goes from being outside the permissible exit cone ϕ to when the ray is inside the cone ϕ. The optimization routines in Zemax try to account for non-smooth merit functions, but performance is greatly improved if the merit function is smoother [42, p. 426]. The principle for this increased smoothness is illustrated in Figure 3.3.

[4] Also known as “cost function” or “objective function” in other optimization literature.

Algorithm 3.1 Pseudocode for desired merit function.

```
for each configuration:
  trace incoming random rays from a 0.27° radius field,
     corresponding to incoming sunlight
  outgoing_energy := 0
  incoming_energy := 0
  for each ray:
    incoming_energy += ray.incoming_energy
    if ray within cone with radius φ:
      outgoing_energy += ray.outgoing_energy
    elseif ray within cone with radius φ+δ:
      outgoing_energy += ray.outgoing_energy * f((ray.angle
         −φ)/δ)}

  efficiency := outgoing_energy/incoming_energy

#optimize for highest possible efficiency for all
   configurations
```

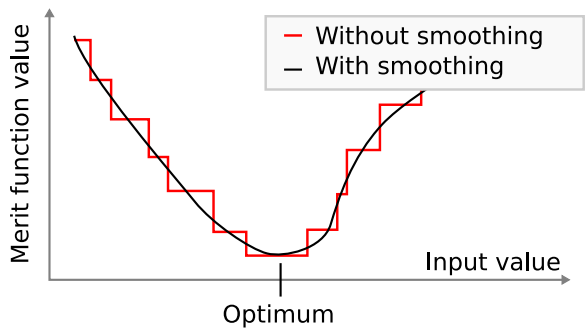

Figure 3.3: Illustration of how the merit function is smoother when the abrubt changes between permissible and not permissible ray angles are removed using the part of Algorithm 3.1 written in bold.

3.4.1.2 Implementing the merit function in Zemax

The pseudo code shown in Algorithm 3.1 must be implemented as a Zemax merit function. This can be done in several ways:

- The Zemax Programming Language (ZPL) can be used to implement it directly. Unfortunately, the performance of ZPL is so low that optimization becomes very slow if it is used to trace the thousands of rays that are needed to generate statistics about system efficiency.

- An external program, written in a language such as C, can be referenced in the merit

function. This was attempted, but in the legacy version of Zemax that was used, there is a significant overhead to using an external program in the merit function. The program is re-run for each iteration of the optimization loop, and must each time it must spend a lot of time on setting up the Dynamic Data Exchange (DDE) communications channel with Zemax.

- The algorithm can be implemented using the optimization operands that are available directly in the merit function editor within the Zemax interface. This has low flexibility, but high performance as it involves neither parsing of an interpreted scripting language, nor communication with an external program.

The merit function was implemented using the optimization operand IMAE [42, p. 401], which traces a number of rays at random position and random field points within a specified field size. The rays are traced through the system, and the operand reports on the percentage of the input energy that reaches the image surface. In order to implement the smoothing of input rays, the image surface is implemented using the built-in Filter4 surface type in Zemax. This surface type has a gradual aperture, where rays are partially vignetted when they are close to the aperture edge. The partial vignetting in the Filter4 surface unfortunately works based on position, not based on angle, and similar functionality is not available for afocal systems. In order to convert angle to position, a large gap is placed between the image surface and the rest of the optical system as shown in Figure 3.4. By adjusting image surface diameter, and gap size L, the permitted angle can be configured. With this configuration, optimization using the IMAE optimization operand works similarily to the pseudocode in Algorithm 3.1.

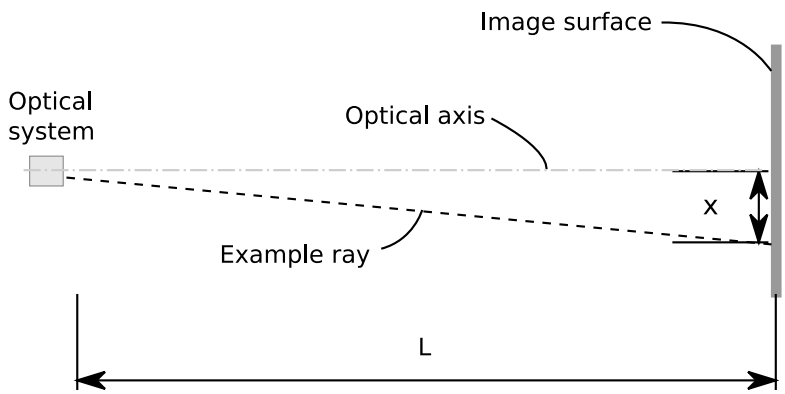

Figure 3.4: Illustration of how exit angle from the optical system is converted to position, for position-based optimization-operands. A ray position x on the image surface corresponds to a ray angle $\phi = \arctan \frac{x}{L}$ when L is large.

Note on a simpler way to go from afocal to focal system In this subsection, converting ray angle to ray position has been done using a large air gap. A simpler solution would have been to convert the system directly to a focal system using a perfect paraxial lens with focal length f to image ray angles onto an image surface. Ray position on the image

surface would then correspond to ray angle according to $\phi = \arctan \frac{x}{f}$, without having to use a large optical gap.

3.4.2 Spectral range

The PMMA model in Zemax is only defined for wavelengths within the range $365\mathrm{nm} \leq \lambda \leq 1060$. The spectrum used for optimization has been a rough approximation of the standard AM1.5D spectrum, clipped to this spectral range.

3.4.3 Multi-level optimization

Each surface is described by a number of aspheric polinomial terms that need to be optimized, in addition to other variables such as lens position and thickness. In total, there is therefore a large number of optimization variables, leading to a large solution space and low optimization performance. In order to improve optimization performance, a multilevel optimization strategy has been implemented, where the optimal shape of the final surface is calculated for each iteration in the optimization loop for the other parameters. This is similar to the concept of a direct "Solve" in Zemax [42, p. 447], in which the curvature or thickness of one surface is automatically adjusted to bring the system into focus. The built-in Zemax functionality only handles the paraxial performance of the system. In our system with large angles, wide aspheric surfaces and multiple configurations, the built-in "Solve" in Zemax is not sufficient.

The implemented multi-level optimization strategy is illustrated in Figure 3.5a. For each iteration of the outer optimization loop, the inner loop calculates the optimal shape of the final surface. Figure 3.5b illustrates which parameters are optimized in the inner optimization loop (green) and which parameters are optimized in the outer optimization loop (red). The inner loop is implemented in ZPL, as will be described next. The outer loop uses the built-in Zemax optimization functionality.

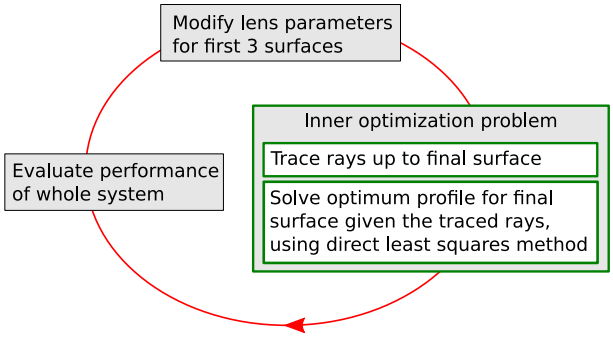

(a) Diagram of the implemented optimizaton procedure.

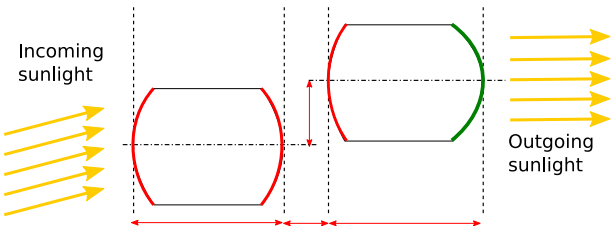

(b) Overview of the variables that are being optimized. The red surfaces and dimensions are part of the outer optimization problem. The green surface is solved directly in the inner optimization problem.

Figure 3.5

3.4.3.1 Inner loop

The inner optimization solution is implemented as a Zemax-macro in ZPL that is run as part of the merit function. The macro performes the following optimization algorithm:

1. Curvatures and thicknesses are read from the $0°$ configuration, and the thick lens equation is used to solve for the curvature on the final surface that gives a paraxial afocal system in this configuration. As a starting point, the final surface is given a parabolic surface profile with the given curvature[5].

2. For each configuration, a number of rays are traced in the meridional plane of the optical system. When the ray number i reaches the final surface, the position y_i and ray angle θ_i is read, as illustrated in Figure 3.6. Using Snell's law and assuming a

[5] A parabolic profile is chosen as an initial profile as it corresponds to the first term of even-termed polynomial that will be used to describe the surface.

lens refractive index of n, the required surface inclination β_i is found:

$$n \cdot \sin(\beta_i - \theta_i) = 1 \cdot \sin \beta_i \tag{3.3}$$

$$\frac{\sin \beta_i \cos \theta_i - \cos \beta_i \sin \theta_i}{\sin \beta_i} = \frac{1}{n} \tag{3.4}$$

$$\cos \theta_i - \frac{\sin \theta_i}{\tan \beta_i} = \frac{1}{n} \tag{3.5}$$

$$\tan \beta_i = \frac{\sin \theta_i}{\cos \theta_i - \frac{1}{n}} \tag{3.6}$$

3. The rotationally symmetric final surface will be described using a polynomial $f(r) = \alpha_1 r^2 + \alpha_2 r^4 + \cdots + \alpha_n r^{2n}$ where n is the total number of terms. Based on the results from the previous step, we have that the desired inclination of the surface at radial distance y_i is: $f'(y_i) = \tan \beta_i$. This can be set up as a linear equation for the polynomial terms α:

$$\tag{3.7}$$

$$2\alpha_1 y_i + 4\alpha_2 y_i^3 + \cdots + 2n \cdot \alpha_n y_i^{2n-1} = \frac{\sin \theta_i}{\cos \theta_i - \frac{1}{n_1}} \tag{3.8}$$

$$\begin{bmatrix} 2y_i & 4y_i^3 & \cdots & 2ny_i^{2n-1} \end{bmatrix} \cdot \begin{bmatrix} \alpha_1 \\ \alpha_2 \\ \cdots \\ \alpha_n \end{bmatrix} = \frac{\sin \theta_i}{\cos \theta_i - \frac{1}{n_1}} \tag{3.9}$$

$$\mathbf{A_i} \alpha = b_i \tag{3.10}$$

4. By combining all the $\mathbf{A_i}$ and b_i terms for all the rays that have been traced in all configurations, we have the following overdetermined linear system:

$$A\alpha = \mathbf{b} \tag{3.11}$$

The system can be solved as a least squares problem, where the optimal polynomial coefficients α fulfill the following equation [43, ch. 6.5]:

$$A^T A\alpha \quad = \quad A^T \mathbf{b} \tag{3.12}$$

Since ZPL does not have a linear algebra library to solve this system, a simple Gaussian elimination algorithm was implemented in ZPL to solve the system for α

5. The lens surface is updated using the newly solved polynomial terms. This changes the surface shape, so the y_i coordinates of Ray's interception point also change. The procedure is therefore iterated starting from the updated surface shape, and it quickly converges.

The optimization problem solved by the inner optimization loop does not directly correspond to the problem solve by the outer loop, for the following reasons:

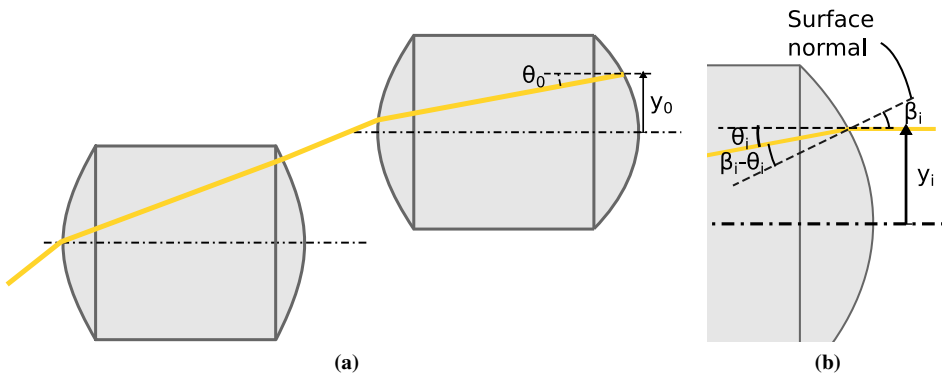

Figure 3.6: Illustration of ray-trace of a single ray, used in the inner optimization loop to find θ and position y (a). Figure (b) is a close-up view and shows relationship between incoming ray angle θ_i and desired surface inclination β_i.

- The inner loop tries to emit all rays with an exit angle of $0°$, but in reality, exit angles of $\pm\phi_{max}$ are acceptable. This is done because it gives a linear system that can be solved very quickly as a linear least squares problem.
- The inner loop considers the sun as a point source, so for a given configuration corresponding to a given incident angle, all evaluated incoming rays are parallel. This is done for simplicity due to the limitations of the ZPL language.
- The inner loop only considers rays in the meridional plane. This might not be representative for all rays, due to astigmatism and the strong asymmetry of the system for high incident angles. This is done for simplicity due to the limitations of the ZPL language.
- The ZPL language is a very slow interpreted language, so in order to keep the performance high, the number of traced rays in the inner loop must be low (on the order of 30-60).

Despite these limitations, the algorithm gives significantly improved optimization performance. By always keeping the system optimally focused in the meridional plane, the outer optimization loop is free to vary the rest of the parameters in order to fulfill the merit function.,

The ZPL macro that implements this inner loop is included in the file 'Zemax/ZPL03.zpl' in the attachments to this thesis. The macro also implements some other functionality that was used during optimization such as restricting the system to a spherical tracking trajectory.

3.4.4 Optimization results

A beam-steering lens array is optimized by using the optimization routines in Zemax combined with the previously described multilevel optimization strategy. The system is opti-

mized over $\pm 40°$ range, with a permitted divergence after the beam-steering lens array of $\pm 2.5°$. Lens material is PMMA, and the system is evaluated using an approximation of the AM1.5D spectrum across the spectral range for which the PMMA data is available in the Zemax Glass Catalog. Tracking is restricted to a spherical path, in order to simplify the kinematics of the structure that will hold the lens arrays.

The resulting lens geometry is shown in Figure 3.7a. The purely geometrical optical system is scale-independent, and can be scaled up or down uniformly in order to create lens arrays with a desired thickness. The individual lenslets have a hexagonal aperture, for close packing in a lens array. The performance of the resulting beam-steering lens array across its field of view is shown in Figure 3.7b, where it can be seen that the divergence half-angle after the the lens arrays is $\leq 2°$. Although this is significantly higher than the inherent $0.27°$, it is below our requirement of $\phi_{max} = 2.5°$ from Section 2.2.6.

The final manufactured geometry is included in the file 'Zemax/Produced_array.zmx' in the attachments to this thesis.

3.4.5 Field curvature and kinematics

In a complete system, the two lens arrays must be attached to a mechanical system that supports translation along the x and y axes, while also controlling the separation along the z axis in order to follow the field curvature. This can be implemented by connecting the two lens arrays using links whose radius is the inverse of the field curvature as illustrated in Figure 3.8. This also prevents rotation about the x and y axes. Translation along the x and y as well as rotation about the z axis can be controlled using three external actuators.

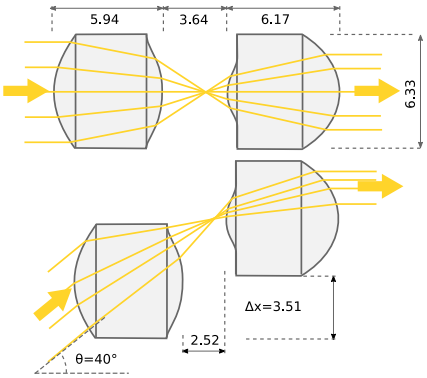

(a) Final geometry of lens arrays, here shown for input angles of 0° and 40°. All length units are millimeters.

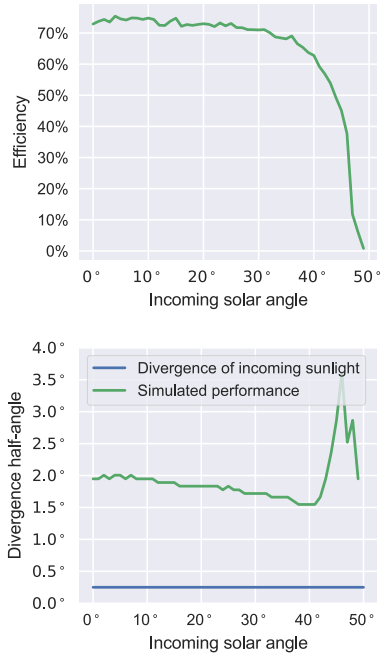

(b) Simulated efficiency of the beam-steering device over its field of view. Divergence half-angle is the the angle at which the beam intensity has reached 10% of maximum intensity, and efficiency is the amount of energy falling within this divergence half-angle. Polarization-dependent fresnel reflection losses are taken into account, while cosine projection loss is not.

Figure 3.7: Optimization results

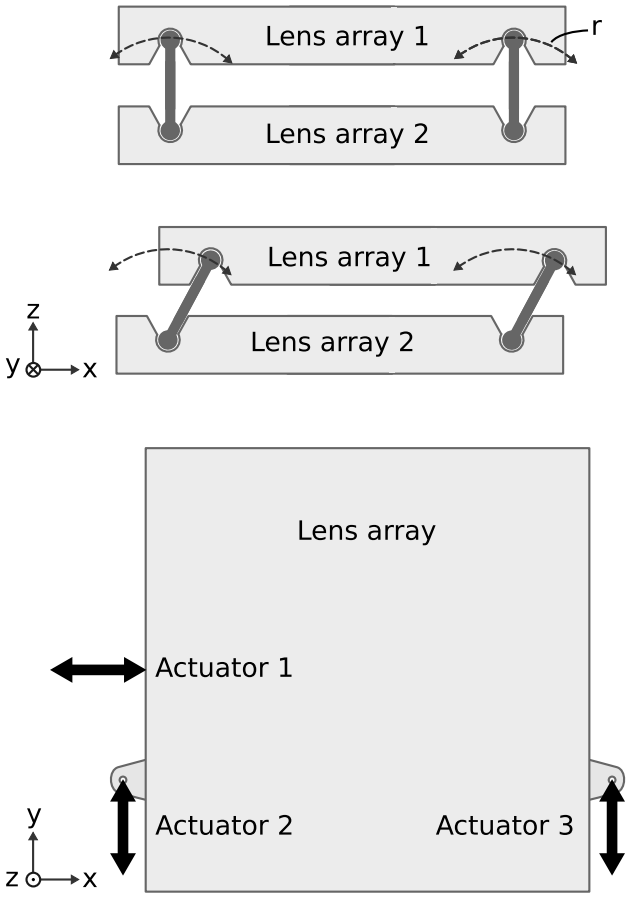

Figure 3.8: Illustration of links and actuators that can be used to control the relative movement of the lens arrays.

Chapter 4

Production of prototypes

A number of prototypes were created during the course of this project, verifying different design principles and concepts. This chapter documents the different prototypes that were created, together with their purposes and the results.

4.1 Experiments with compression molding of transparent polymer plates

Thermoplastic optics can be manufactured using a number of production techniques, including:

Hot embossing: Using a patterned mold to emboss lens surfaces onto a heated plate of the lens material. Especially useful for micro-optics.

Injection molding: Material is heated and injected into a mold under high pressure, where it cools and solidifies. High set-up costs but very low cycle times and tight tolerances [44, p. 278].

Compression molding: Placing pre-heated material directly into a mold, after which the two mold halves are pressed together. This has low set-up costs and is useful for prototyping, but cycle times are long and tolerances can not match injection molding [44, p. 289].

Compression molding was considered a promising solution for prototyping. The process is easy to prototype and allows complicated and aspherical optical designs. For high volume production, related techniques such as injection molding can be utilized.

In order to gain experience with the process, a number of lenses were compression molded by hand with 3D printed molds. The molds were 3D printed in PETG on a FDM 3D printer. The lenses were molded from PMMA and SAN plates, commercially available through the retail hardware stores Clas Ohlson and Biltema. The results were best from SAN, due to its low glass transition temperature. This was important when compression

molding by hand using 3D printed molds, because it is important that the 3D printed mold is not heated to the point where the mold is deformed instead of the lenses. Some photos of the process are shown in Figure 4.1.

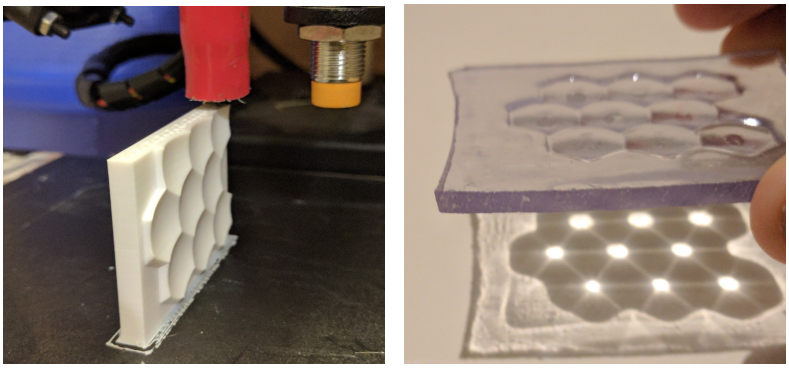

(a) 3D printing of mold for experimenting with lens production

(b) First test of compression molded lens array showing array of images of a distant light source

Figure 4.1: First tests of compression molded lenses

4.2 First test of the beam-steering lens array principle

When the concept of beam-steering lens arrays materialized as a possible solution, a small prototype was made with the purpose of demonstrating the principle. A lens design was created in Zemax and optimized for $\pm 35°$. Molds based on this lens design were 3D printed, and SAN plates were molded into small lens arrays.

The lens arrays consisted of 3x4 lenslets. The accuracy of the replication was low due to the small sizes of the lenslets and imprefections when 3D printing, but the resulting lens arrays were able to demonstrate the concept. The lens arrays were attached to a 3D printed frame fixed to the correct position for steering a beam with a $12°$ incident angle.

Due to the small size and low accuracy of the prototype, no efficiency measurements were performed. Some photos of the prototype can be seen in Figure 4.2

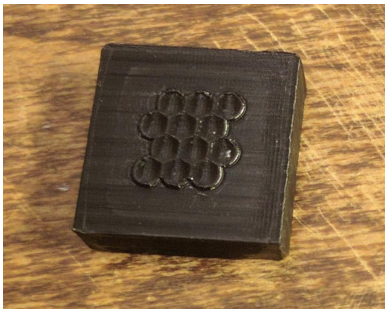

(a) One of the molds for the first beam-steering lens array prototype

(b) Assembled lens array prototype

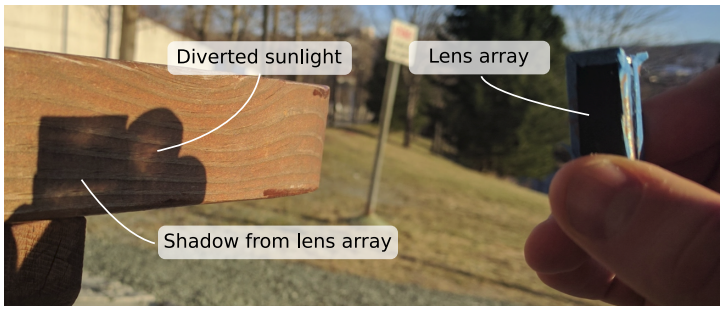

(c) Lens array prototype demonstrated in sunlight

Figure 4.2: First test of beam-steering lens array principle

4.3 Manually controlled beam-steering lens array

After developing the beam-steering concept further, a manually controlled beam-steering prototype was created in order to verify and demonstrate the principle.

4.3.1 Lens array

The lenses for the prototype were optimized for $\pm 30°$ acceptance angle, and they were simulated to have $> 70\%$ efficiency over this field of view. The arrays consisted of $5\mathrm{mm}$ diameter lenslets, arranged in a $50\mathrm{mm} \cdot 50\mathrm{mm}$ array. The arrays were compression molded from Styrene-Acrylonitrile (SAN) plates in a 3D printed mold. SAN was chosen because it is easily molded in 3D printed molds. Molding was done by hand, by heating the SAN plates with a heat gun to approximately $150°C$ before placing them in the mold. A mechanical lever was used to reach a molding force of approximately 1kN.

4.3.2 Tracking kinematics

Tracking is accomplished by lateral translation of the two lenslet arrays. In order to get good tracking, their vertical separation also need to be controlled in order to follow the

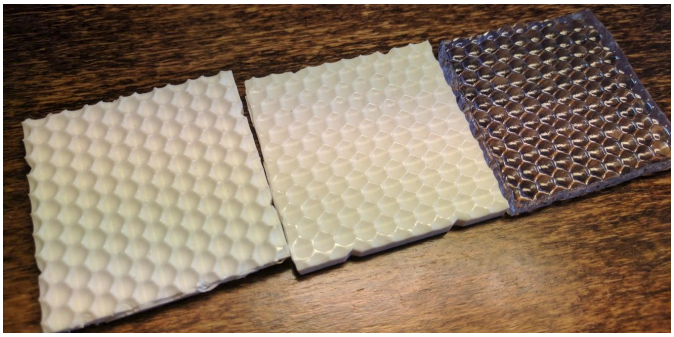

Figure 4.3: Parts of the mold for the manually controlled beam-steering lens array

field curvature of the system, as explained in Section 3.4.5. In order to accomplish this, the arrays are joined by links that have the same length as the radius of the field curvature. These links are shown in yellow in Figure 4.4, and they are connected so that the relative movement between the arrays is limited to translation in the x and y direction.

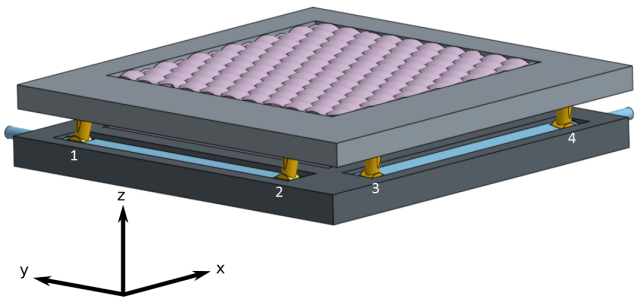

Figure 4.4: Tracking mechanism for the manually controlled beam-steering lens array. The yellow links connect the two arrays. The blue bars connect rotation about the y axis for link 1 and 2, and rotation about the x axis for link 3 and 4. These connections lock the arrays against rotation about the z axis.

4.3.3 Reflector

The beam-steering lens array was attached to a 3D printed holder and parabolic reflector with a shape inspired by the sketch in Figure 2.2. The reflector was made by 3D printing the parabolic shape, sanding it down to a smooth surface, and attaching reflective aluminized polyester tape to the surface.

The mechanical CAD software Onshape was used for the design of the 3D models. At the time, Onshape did not have native support for conic curves, so an extension was written using the Onshape programming language Featurescript, in order to easily generate 3D models with parabolic surfaces. This extension is described in Appendix C.

4.3.4 Results

The prototype demonstrated the beam-steering principle, and how it could be used for controlling the position of a focal spot. A video demonstration of the prototype is available in the attachments to this thesis, with the file name 'demonstration_manually_controlled.mp4'. The video is also available on the web, at https://goo.gl/photos/NnLbPxVNbTavEKsZ6.

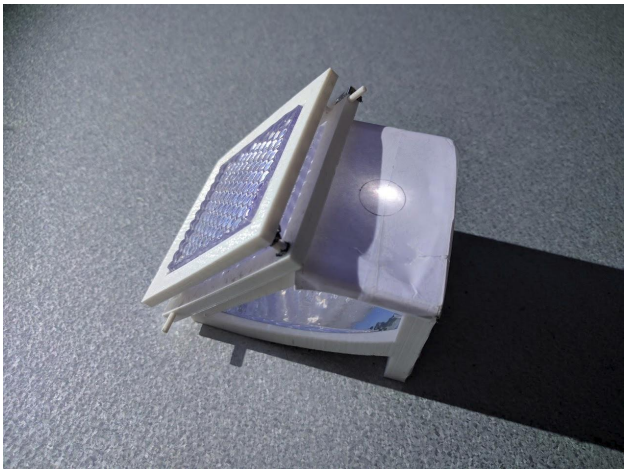

Figure 4.5: Manually controlled beam-steering lens array tested in the sun.

Approximate performance measurements were performed on this prototype, using image analysis from raw photos of the focal spot. This analysis is described in Appendix D. The analysis indicate a concentration factor of approximately 7x and approximately 15% efficiency of the complete system. Losses in different parts of the system have been measured and estimated in order to explain the low overall system efficiency:

- 30% loss due to Fresnel reflection losses and aberrations, simulated in Zemax.
- 20% loss due to absorption losses in the SAN plates, measured through image analysis.
- 50% loss in the reflector, measured through image analysis.
- 20% loss due to incomplete lenses around the edges of the small lens array.

Together, this gives a predicted efficiency of $\eta_{predicted} = (1 - 0.3) \cdot (1 - 0.2) \cdot (1 - 0.5) \cdot (1 - 0.8) \approx 22\%$. Much of the remaining losses can likely be explained by excessive divergence of sunlight after passing through the lens arrays, due to the low precision of the FDM 3D printed molds.

4.4 Automatically controlled beam-steering lens array

After demonstrating the principle of beam-steering lens array, a new prototype was created in order to increase performance and include automatic motorized tracking. PMMA was

used as lens material in accordance with the discussion in Section 3.3.

4.4.1 Lens array

The lenslets described in Section 3.4.4 with $\pm 40°$ acceptance angle were assembled into a $72\text{mm} \cdot 72\text{mm}$ lens array.

Tolerance analysis on the resulting system was carried out using tolerancing functionality in Zemax in order to prepare the system for production. Molds were milled from aluminum in MTP Realiseringslab as shown in Figure 4.6, and compression molding was performed in in MTP Plastlab with a Fontijne hydraulic platen press with integrated heating as shown in Figure 4.7.

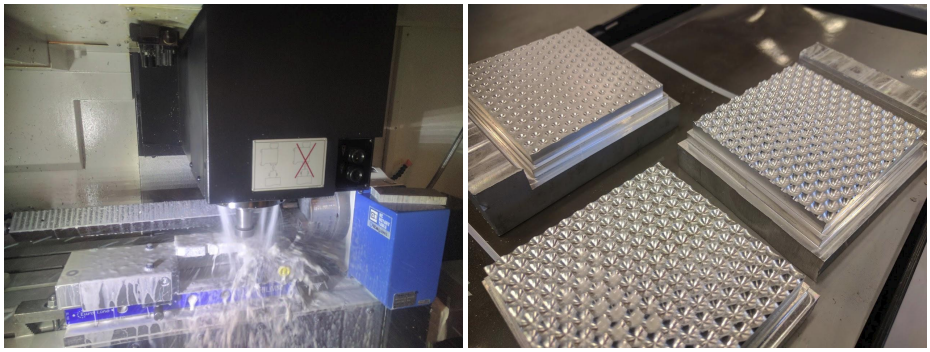

Figure 4.6: CNC milling of aluminum molds

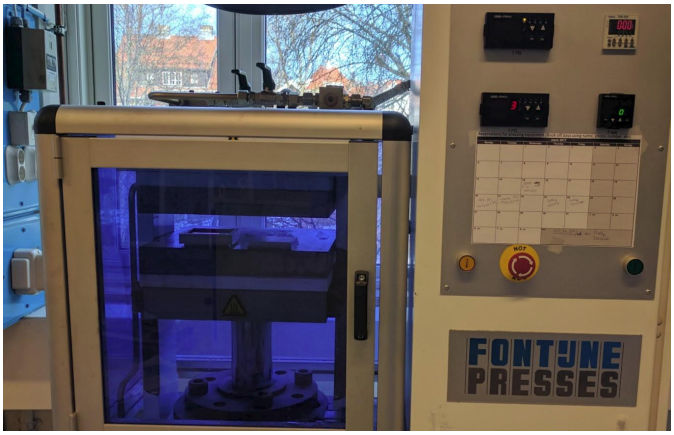

Figure 4.7: Molds and PMMA plate inside the Fontijne hydraulic platen press.

When compression molding the lens arrays, the geometry inherently causes air to be trapped at each lenslet surface. As a simple work-around during prototyping, air bubbles were allowed to escape by temporarily cooling the mold and removing the holding pressure: After the first iteration, the lenses were slightly flat at the top due to the trapped air,

but after the second iteration, no air bubbles were visible. The process is illustrated in Figure 4.8

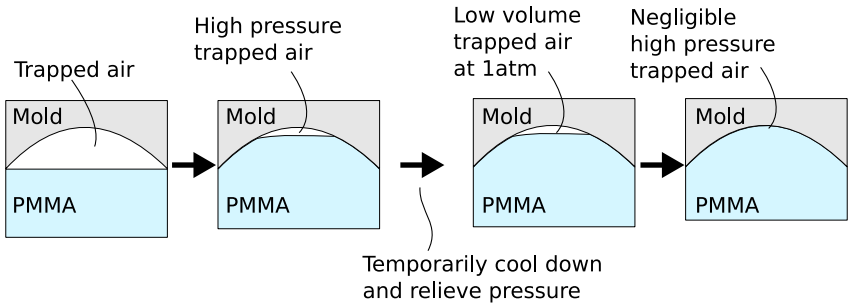

Figure 4.8: Principle of removing air bubbles by repeated pressing.

The surface quality after pressing was not very good. Optical clarity was improved by polishing the resulting lenses with a polishing compound and a buffing wheel, but there appeared to be some surface waviness with a wavelength of about 100-200μm based on a visual inspection as is visible in Figure 4.9. The same waviness appears to be present in the molds, so it is likely a result of the machining process. Accurate profiling of the surface has not been carried out.

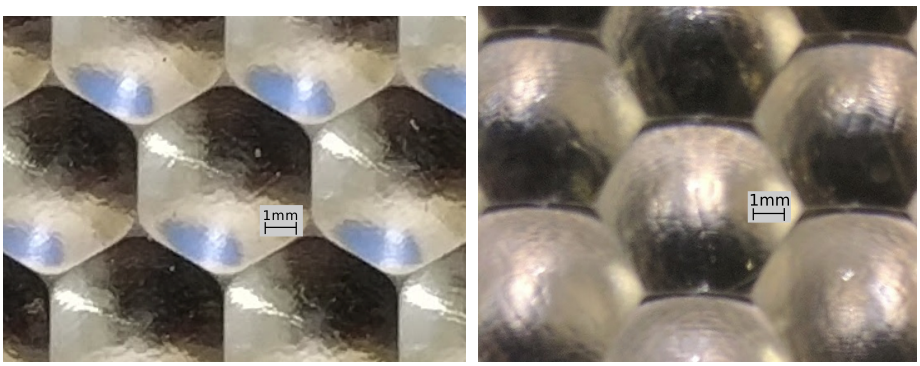

(a) **(b)**

Figure 4.9: Close-up view of mold (a) and lens array (b), showing the surface waviness.

4.4.2 Direction sensor

Sensing of solar position was implemented using a set of four photocells, each inclined $\pm 40°$ from the front plane about its respective axis. The projected area of each photocell depends on its angle, so the photocell pointing towards the sun receives more total flux than the one pointing away, as illustrated in Figure 4.10.

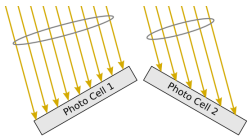

Figure 4.10: The cosine projection effect: The incident flux on photocell 2 is lower than that on photocell 1.

A photo cell is a light dependent resistor, where there is a power-law relationship between the illuminance E_v and the resistance R:

$$\frac{R}{R_0} = \left(\frac{E_v}{E_{v0}}\right)^{-\gamma} \tag{4.1}$$

For an inclined photocell, the illuminance is proportional to the cosine of the angle between the solar radiation θ and photocell inclination ϕ. By combining solar flux density, R_0 and E_{v0} into a constant k, we have the following relationship:

$$R = k \cdot (\cos(\theta - \phi))^{-\gamma} \tag{4.2}$$

If two photocells that are inclined in opposite direction are connected in series as a voltage divider, the middle voltage is:

$$V = V_0 \cdot \frac{R_2}{R_1 + R_2} = V_0 \cdot \frac{(\cos(\theta - \phi_2))^{-\gamma}}{(\cos(\theta - \phi_1))^{-\gamma} + (\cos(\theta - \phi_2))^{-\gamma}} \tag{4.3}$$

The resulting voltage is independent of k and only depends on the relative angles. Therefore, the solar angle can be estimated by reading out this voltage, independent of the current sunlight intensity. A circuit implementing this principle is shown in Figure 4.11a, where an additional series resistor has been added in order to be able to measure the total flux density. The 3D printed holder for the inclined photocells is shown in Figure 4.11b.

Photocells were chosen because they were readily available and because the voltage divider setup allows measurement over a wide dynamic range with few low-resolution ADC-inputs. However, photocells are not ROHS compliant, they are fairly temperature dependent, and they do not perfectly follow the given power law. In a complete implementation, a phototransistor would therefore likely be used instead of a photocell due to its high linearity and its ROHS compliance.

4.4.3 Controlling the lens arrays

Lateral translation of the lens arrays is implemented using two TowerPro SG92R micro servos connected as shown in Figure 4.12a. The motion is restricted using the links shown in Figure 4.12b similar to the links for the manual prototype shown in Figure 4.4. An Arduino Nano is used to read the sensor data and control the servos.

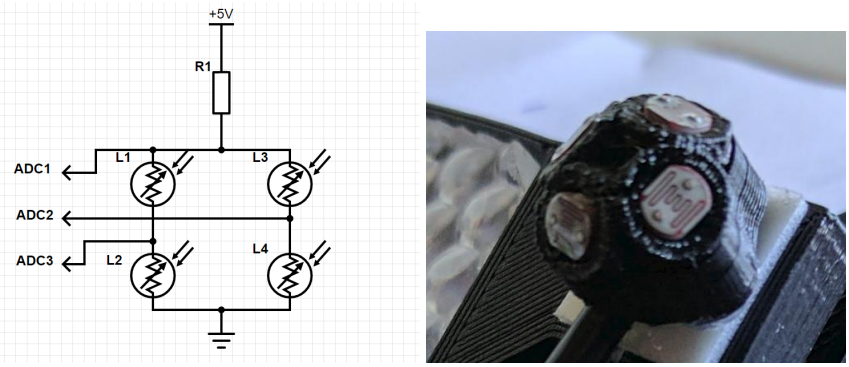

(a) **(b)**

Figure 4.11: Schematic of solar direction sensor (a) and assembled direction sensor (b)

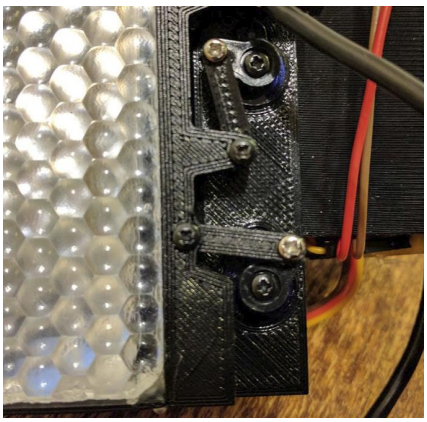

(a) Two micro servos with links connecting them to the top lens array.

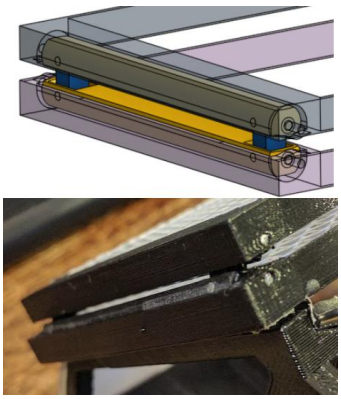

(b) Links that kinematically lock the lens arrays to motion in the desired directions

Figure 4.12: Mechanisms that implement relative movement between the lens arrays.

4.4.4 Closed-loop control

The direction sensor described in Section 4.4.2 is not completely accurate. It assumes that all incident flux comes directly from the sun, so it can be affected by bright surroundings. In addition, there is some hysteresis in the movement of the lens arrays, due to imperfect joints and imperfect links between the servos and the lens arrays. Closed-loop control must therefore be used for the final adjustment.

Initial test using single sensor A single photo diode with a very narrow acceptance angle was placed behind one of the lens pairs in order to detect the error in the angle of the transmitted light. An orthogonal descent optimization algorithm was tested, but acceptable

performance was not reached:

- It was difficult to perfectly orient the photo diode within the $< 1°$ degree tolerance required for the system to hit the right focal spot.
- When the system is too far away from the target, no light hits the photo diode within its narrow acceptance angle. This leads to a flat area in the cost function, which the optimization routine struggles to handle.
- The hysteresis of the movement of the lens arrays makes it difficult to perform the small movement to detect descent direction.

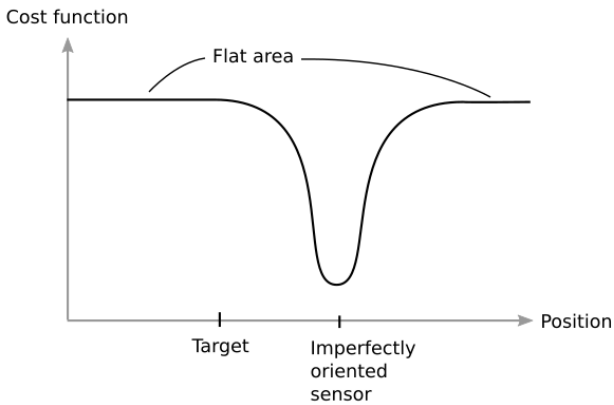

Figure 4.13: Qualitative illustration of the problems with the current sensor for closed-loop control

Second test using four sensors In order to improve the performance of the closed loop control, a small fraction of the solar energy is redirected to a second focal spot next to the main one as shown in Figure 4.14. Here, the light hits an array of four photocells that are used to close the loop for the control algorithm. The feedback from the photocells is connected to the control loop using an integral term. In order to prevent the control loop from becoming stuck in a local minima far away from the correct solution, the integral term has a maximum value of $5°$, and it is automatically reduced when large changes in solar angle is detected. Faster and more robust performance can likely be achieved using a more complex and better tuned control algorithm.

4.4.5 Secondary reflector

A simple secondary reflector has been designed according to the principles described in Section 2.2.7, and has been included in the prototype. Due to time constraints, a more detailed and optimized secondary reflector has not been constructed.

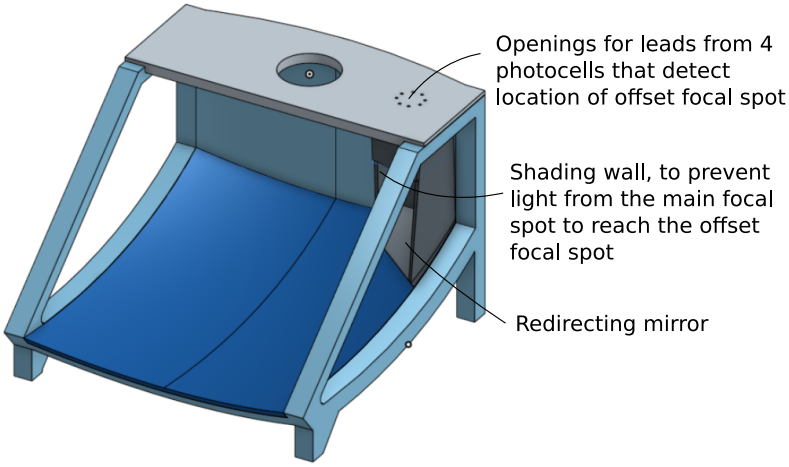

Figure 4.14: 3D model of the hardware for closed-loop control, where a small part of the sunlight is redirected to a second focal spot hitting an array of 4 photocells.

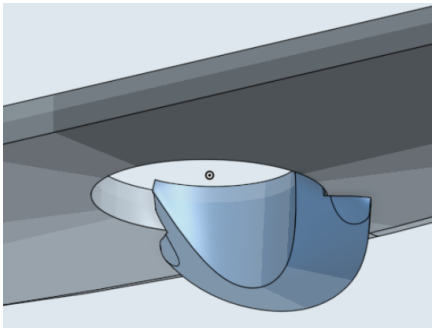

Figure 4.15: 3D model of simple secondary reflector attached to underside of the cooker's top-plate.

4.4.6 Demonstration in the sun

A live demonstration of the proof of concept with open loop control is available in the attached video 'demonstration_openloop_control.mp4'. A video of the improved performance after closing the loop is available in the attached video 'demonstration_closedloop_control.mp4'. The videos are also available on the web at https://goo.gl/photos/NnLbPxVNbTavEKsZ6.

Figure 4.16: Testing the device outdoors in the sun. Videos are available at https://goo.gl/photos/NnLbPxVNbTavEKsZ6

4.4.7 Performance

Detailed analysis of the lens array has been performed using image analysis techniques that are outlined in Appendix D, and overall performance of the assembled system has also been performed.

4.4.7.1 Beam-steering lens array

The two most important performance indicators for beam-steering lens arrays are transmission efficiency and divergence half-angle after the array. Efficiency is important in order to keep the efficiency of the complete system high, and divergence half-angle is important in order to allow for high concentration in the concentrator that follows the beam-steering lens arrays.

These performance indicators were measured from the beam-steering lens array prototypes with the test setup described in Appendix D.

From the results in Figure 4.17, it can be seen that the resulting lens arrays have $\approx 75\%$ increased divergence compared to the simulation results. The divergence half-angle is still mostly below the $3.5°$ limit calculated in Section 2.2.6, but not below the $2.5°$ limit that was chosen in order to allow for inaccuracies in the parabolic mirror. The main reason for the increased divergence is most likely the low surface quality, as can be seen in Figure 4.9. With improved manufacturing of the lens array, especially with improved surface quality of the mold, the performance is expected to approach the simulated values.

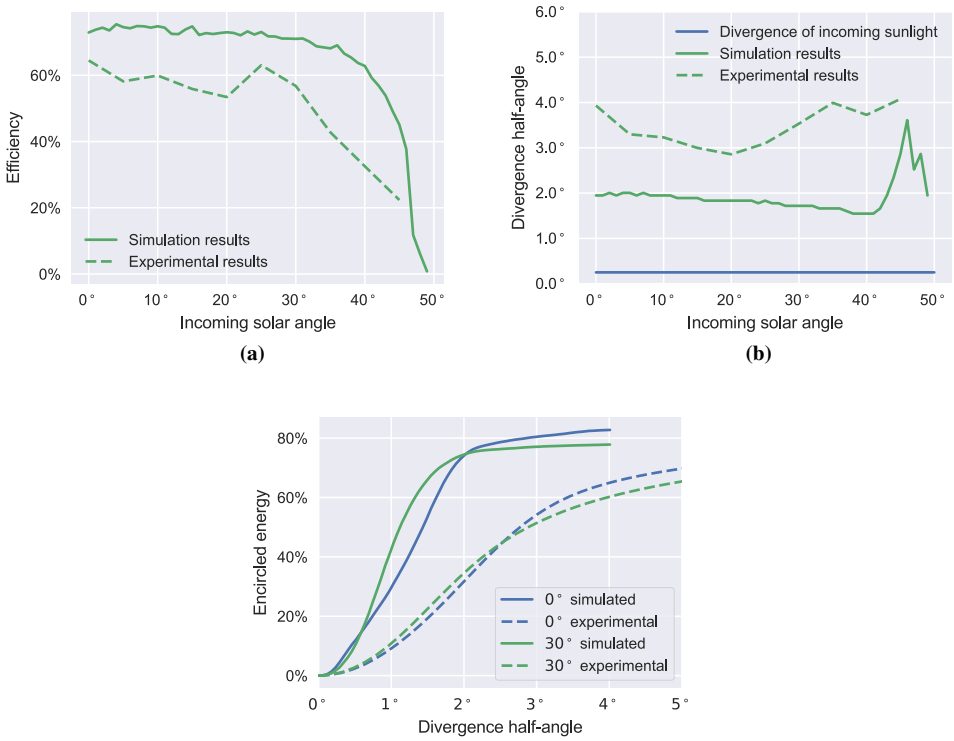

Figure 4.17: Efficiency (a), divergence (b) and encircled energy (c) plots of the bare beam-steering lens array. Divergence is defined as the divergence angle where intensity has fallen to 10% of maximum intensity, and efficiency is the amount energy falling within this divergence angle. Fresnel reflection losses aretaken into account, while cosine projection loss is not.

4.4.7.2 Performance of complete system

In order to evaluate the performance of the complete prototype, the size of the cooking surface must be scaled down by the correct scaling factor.

The prototype has an array size of $A_{prototype} = 72\text{mm} \cdot 72\text{mm}$. Uniform scaling gives a cookware diameter of: $D_{cooking,prototype} = D_{cooking} \cdot \sqrt{\frac{A_{prototoype}}{A}} = 180\text{mm} \cdot \sqrt{\frac{72\text{mm} \cdot 72\text{mm}}{1000\text{mm} \cdot 1300\text{mm}}} \approx 11.4\text{mm}$. This means that a target diameter of 11.4mm must be used, to correspond to a target diameter of 180mmin a scaled-up cooker. Image analysis has been used to evaluate the performance of the complete prototype, measuring the amount of energy falling within this diameter. Test setup is explained in Appendix D. These results are compared with the performance of the bare parabolic reflector (manually aimed towards the sun), and shown in Figure 4.18.

The low efficiency of the completed prototype is likely due to a combination of several factors:

- The bare parabolic mirror is created by attaching reflective film to a parabolic surface. The resulting reflector has a number of surface errors, leading to large spreading of the focal spot even without lens array.
- The surface errors in the lens arrays lead to increased divergence compared to simulated values. Combined with the spreading from the parabolic mirror, this causes a significant portion of the energy to be spread outside the target area.
- The mechanism that prevents rotation about the z axis, as shown in Figure 4.12b, has too much backlash so that the lens arrays are not perfectly lined up. In order to prevent this, a third actuator should have been used instead, as described in section 3.4.5.

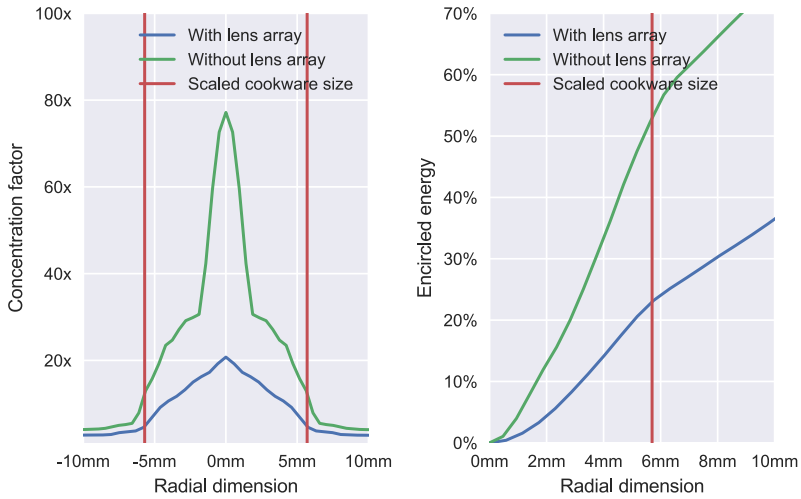

Figure 4.18: Measured efficiency of complete prototype, compared to performance of the bare parabolic mirror without beam-steering lens array.

4.4.7.3 Thermal efficiency measurements

In order to test the performance across the whole solar spectrum and verify the performance predicted by image analysis, a separate test was performed by heating a known quantity of water on the prototype.

A $7\mathrm{ml}$ water container was 3D printed with a $400\mu\mathrm{m}$ thick, $\varnothing 12\mathrm{mm}$ target surface. Temperature measurements inside this container were performed using an active thermistor connected to an Arduino development board.

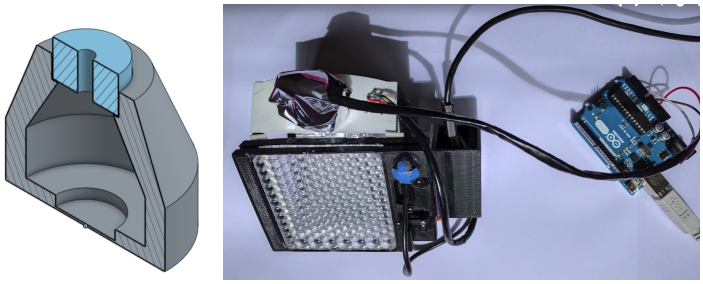

(a) Section view of $7\mathrm{mL}$ water container

(b) Complete system during testing.

Figure 4.19: Test setup for measuring thermal efficiency of the system.

A complete cycle was captured where the water was heated from $25°C$ to $42.5°C$ using solar energy on the cooker prototype cooker. Thereafter, the system was allowed to cool back down by placing a shading surface in front of the prototype cooker.

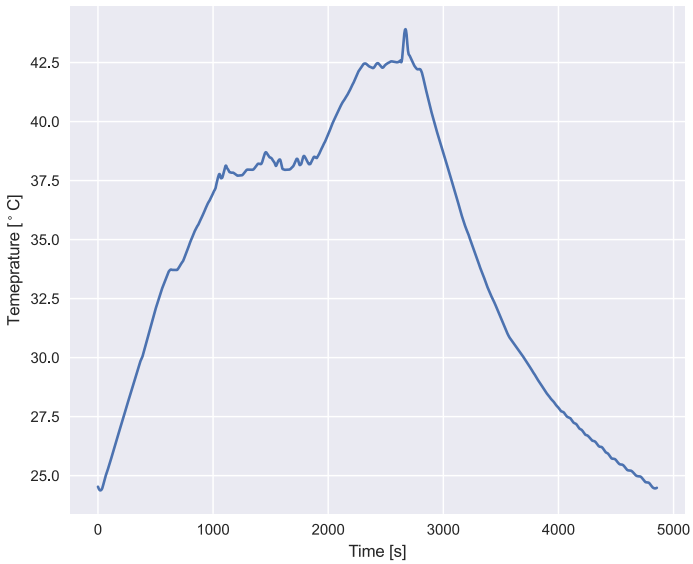

Figure 4.20: Temperature measurements when heating $7\mathrm{mL}$ of water on the cooker, and letting it cool back down in the shade. The two flat areas of the plot are likely due to the control system struggling to keep the system completely in focus due to the backlash in the mechanism that prevents relative rotation about the z axis. Test performed at 2017-06-08 during the time-period 17:25-18:45. Weather: partly cloudy, clouds not covering the sun.

The rate of temperature change can be converted to heat flux by considering water's heat capacity: $\dot{Q} = m \cdot C \cdot \frac{dT}{dt}$ where $\dot{Q}$ is sum of heat fluxes to the water in the container. Conservation of energy gives that $\dot{Q} = \dot{Q}_{sun} + \dot{Q}_{ambient}$ where $\dot{Q}_{sun}$ is heat flux provided by the solar energy, and $\dot{Q}_{ambient}$ is heat flux from the abient environment (typically a negative value due to heat loss). This means that by measuring $\dot{Q}$ and $\dot{Q}_{ambient}$, the value of $\dot{Q}_{sun}$ can be estimated: $\dot{Q}_{sun} = \dot{Q} + \dot{Q}_{ambient}$. In order to visualize this, heat flux is plotted against temperature across the complete heating and cooling cycle, as shown in Figure 4.21. By reading the vertical separation between these lines, approximate $\dot{q}_{sun}$ can be measured. Visual inspection gives a vertical separation of approximately $0.75W$[1]. For the $72\text{mm} \cdot 72\text{mm}$ area of the beam-steering lens array, this translates to a power density of $\frac{\dot{q}_{sun}}{A} = \frac{0.75\text{W}}{72\text{mm} \cdot 72\text{mm}} \approx 155\text{W}/\text{m}^2$. The intention was to compare this to measured solar irradiance values, but the solar irradiance measurement equipment at NTNU is out of order so this could not be done. Comparison to the AM1.5D standard of $900\text{W}/\text{m}^2$ gives a very approximate efficiency value of $\eta \approx \frac{155\text{W}/\text{m}^2}{900\text{W}/\text{m}^2} \approx 16\%$. This is significantly lower than the $\approx 23\%$ efficiency measured using image analysis in Section 4.4.7.2. The lower efficiency can have a number of reasons:

- Real solar irradiance might have been much lower than $900\text{W}/\text{m}^2$.
- When performing image analysis, a visuall inspection is performed to ensure that the beam-steering lens array is perfectly tracked. For thermal measurements, all tracking is performed by the control system. The backlash when it comes to rotation about the z axis might cause this tracking to sometimes be imperfect. Due to time limitations at the end of the master's, there was not enough time to tweak the control system to improve tracking accuracy.
- The 3D printed water container was manually placed over the focus opening in the top plate of the solar cooker, and was not necessarily perfectly centered.
- The image analysis only measures performance in the visible spectrum. Performance outside the visible spectrum might be lower, leading to lower total performance.
- The methods used for image analysis are very uncertain, as explained in Appendix D.6.1 on page 88.

4.4.8 Lessons learned from prototype

A number of lessons were learned from this prototype, which will be useful in future developments of the product:

- It is difficult to achieve the required tolerances using only two actuators. Instead, three actuators should be used, as described in Section 3.4.5.

[1] Due to the lack of solar irradiance measurements to compare the value to, more accurate readouts using linear regression has not been performed.

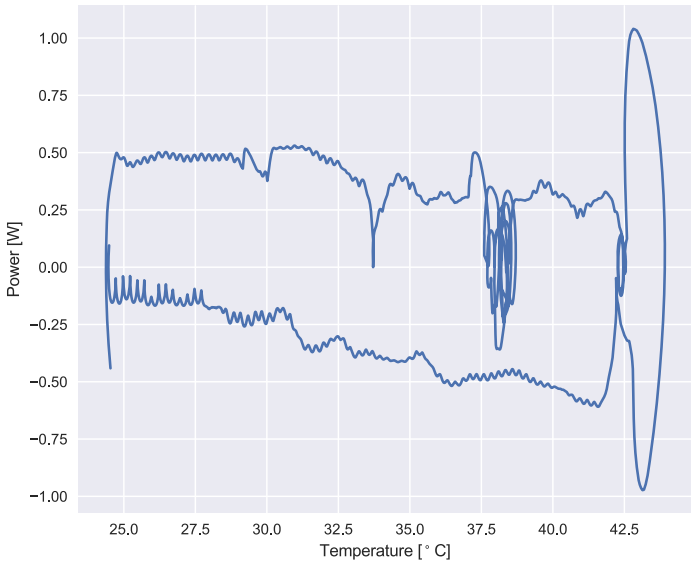

Figure 4.21: Heat flux versus temperature for the complete heating and cooling cycle. The top line is from the heating cycle and represents $\dot{q}$. The lower line is from the cooling cycle and represents $\dot{q}_{ambient}$.

- The accuracy of the parabolic mirror is important for overall system efficiency, and greater focus must be placed on manufacturing a high-quality parabolic mirror.
- There are strict tolerances for separation between the lens arrays, so a mechanism for adjusting this distance during lens array assembly should be implemented.
- Surface quality of the existing process is not good enough, and molds with increased surface quality must be produced. Optimally, this should be done using single-point diamond milling on a precision mill.

Chapter 5

Turning it into a usable product

The concept of a solar cooker based on a beam-steering lens array has been demonstrated on a small scale, as reported in Chapter 4. The existing prototypes have demonstrated that the system works as expected on a small scale. In order to turn the proposed concept into a working, commercializable product, the power must be scaled up several orders of magnitude from the prototypes. This chapter argues for how the concept can be scaled up, and what kind of benefits will be achievable for a product based on an up-scaled version of the concept.

5.1 Geometric scaling effects

The concept illustrated in Figure 2.2 can be split into two parts: beam-steering lens array, and reflector with frame. The reflector is a scale-independent geometrical optical system. In order to increase cooking power, this system can be scaled uniformly. The beam-steering lens array on the other hand, can be scaled by increasing the size of the array, keeping the size of each individual lenslet constant. In this way, tracking is implemented using the same millimeter-scale lateral translation even for meter-scale arrays.

The fact that the size of the tracking motion remains constant as the system scale is increased illustrates one of the benefits of beam-steering over traditional solar tracking: The amount of inertia to overcome by the tracking system is reduced. For lateral translation, the actuator needs to move the inertial mass m. If the thickness is assumed to be constant, tracking inertia is proportional to area:

$$m = \rho V \propto A \tag{5.1}$$

If the whole reflector is to be rotated, as in traditional solar tracker, the tracking actuator must overcome system's mass moment of inertia. The mass moment of inertia is proportional to mass multiplied by the square of a system dimension. If the thickness is assumed to be constant, this means that tracking must overcome an inertia that is proportional to the square of the area:

$$I = \int\int\int \rho r^2 dV \propto mL^2 \propto A^2 \tag{5.2}$$

For this reason, the power requirements required for beam-steering tracking increase approximately linearly with area, while power requirements for traditional tracking increases approximately with the square of the area. In the prototypes, this tracking power is provided by a rechargeable battery. In a commercial product, this can be combined with a small PV element, so that it does not need to be manually recharged. Future developments of the beam-steering lens array may also allow passive tracking due to the small movements, low inertia and low friction of the system.

5.2 Production techniques

For prototype production, compression molding has been used due to its simplicity. This has a fairly slow turnover rate, and is not very suitable to mass production[44, p. 287]. However, other high turnover rate techniques, such as injection molding, can be used for mass production of a commercialized system. In order to limit tooling and mold costs, a smaller mold might be used in order to produce smaller lens arrays which are tiled into a larger array on a large solar cooker. This will be a trade-off between tooling costs and assembly costs, as tiling lens arrays requires more steps during production, especially ensuring that the tiles are aligned within the strict tolerances.

Several different production techniques are possible for the parabolic reflector. For mass production, either anodized aluminum mirror or a molded aluminum-coated PMMA mirror is likely a good choice. For prototypes and low-volume production, reflective film can be attached to 3D printed, milled or laser cut surfaces.

Unlike traditional solar cookers, a beam-steering lens array solar cooker can not easily and cheaply be produced from off-the-shelf materials. This prevents immediate production of low-cost versions of the concept. It does however lend itself to volume production, which could bring down the unit cost over time. The increased user friendliness, as will be discussed in Section 5.4, might increase the market size to the point where high volume production can bring down the unit price.

There are also other use cases for a beam-steering lens array, where a combination of use cases might help developing and maturing the concept, in order to bring down unit cost:

- Steerable LED lights.
- Solar Lighting systems for steerable natural illumination.
- Solar tracking for CPV concepts that lack integrated tracking, such as Morgan Solar SunSimba [45].
- Medium-scale solar-thermal industrial processes.

5.3 Tolerances

The tolerances for the beam-steering lens array are on the order of $100\mu\mathrm{m}$ for relative position and even stricter for the surface profile. Scaling up a system makes it more difficult to maintain such a strict tolerance due to a number of effects such as thermal expansion, elastic deformations and accuracy of tooling. However, several aspects of the nature of a beam-steering lens array makes the system less susceptible to the problems of scaling up:

- Surface quality is a function of mold quality. Manufacturing a mold with high surface quality is a slow process, but this is a one-time cost.
- Thermal expansion affects the upper and lower lens array by the same amount, so the lens arrays can be kept aligned despite changes to their dimensions through thermal expansion. For the z-axis, the distances are much shorter so relative tolerance if fairly loose and thermal expansion is not a problem.
- Actuators are connected to sensors for the transmitted light using closed-loop control, so the arrays will be translated to their best possible alignment despite inaccuracies during assembly.
- In order to prevent plate bending from changing the separation between the lens arrays along the z-axis, z-links can be distributed at regular intervals across the surface.

These principles are illustrated in Figure 5.1.

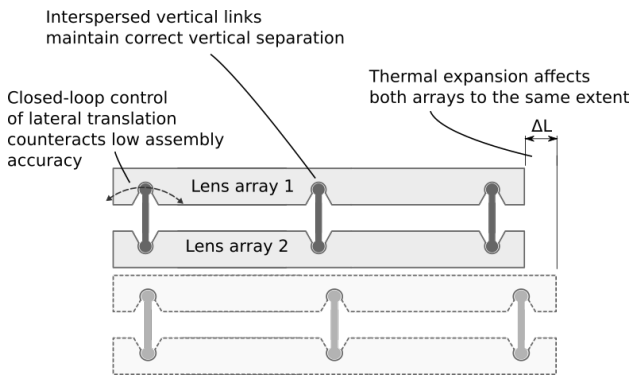

Figure 5.1: Illustration of principles that are used to maintain strict tolerances despite scaling up the system

5.4 User friendliness

The main benefit of including beam-steering in the solar cooker is increased user friendliness. The user simply places the cooker outside, pointing in the general direction of the

sun, and the cooker handles the rest. A tracking range of $\pm 40°$ gives up to 5hours and 20 minutes unattended tracking:

$$\frac{2 \cdot 40°}{15°/\mathrm{h}} = 5.33\mathrm{h} \tag{5.3}$$

With this tracking range, full-day cooking in equatorial regions can be achieved with only two distinct cooker orientations, as illustrated in Figure 5.2. Closer to the poles, the distinct cooker orientations are necessarily different, but the same principle of pointing in the general direction of the sun still applies. If the solar cooker is optimized for regions far away from the equator where the sun never reaches zenith, the inclination of the lens arrays can be increased in order to increase efficiency at lower solar elevation.

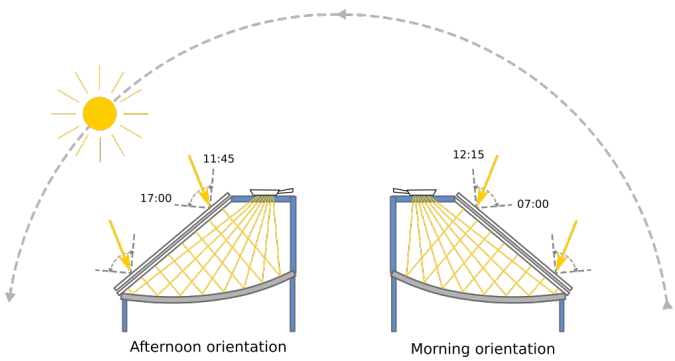

Figure 5.2: Illustration of how a beam-steering solar cooker wiht $\pm 40°$ acceptance angle can be used throughout the day in only two distinct orientations, illustrated for equatorial regions with the sun near zenith at midday.

The automatic fast tracking also enables other functionality that can increase the user friendliness and safety over a conventional parabolic solar cooker:

- Cookware detection can be implemented, where the beam-steerer is quickly defocused if no cookware is detected, in order to protect the users from the concentrated solar energy.
- Adjustable cooking power can be implemented by pulse-width modulation of focused and defocused beam-steering lens array.
- An infrared temperature sensing module can detect the temperature of the cookware, in order to prevent dry-cooking or burning food.[1]
- The fixed position of the parabolic mirror allows the use of protective surfaces that separate the user from the concentrated sunlight.

[1] This must be calibrated to the emissivity of the surface of the cookware. However, a cooker would likely be sold with corresponding cookware in order to utilize surface material with high absorbtion of solar energy, and preferably low emissivity for long-wave infrared radiation.

5.5 Combination with heat storage and transport

For a direct solar cooker, there is a trade-off between cooking power and cooker size, as illustrated in Figure 2.3. One way to circumvent this trade-off while still benefiting from the beam-steering solar tracking could be to integrate the concept with heat storage and transport:

- A heat transfer medium or optical light guide could transfer energy from a large, fixed solar concentrating appliance placed outdoors to an indoor cooking surface
- By using a heat storage medium, the appliance can be allowed to collect energy throughout the day, allowing for high cooking power without an excessively large receiver.

In order to limit the scope of this thesis, further evaluation of the possibility of integrating heat storage and transport has not been performed. Other variants of heat storage and transport have previously been explored at NTNU, with mixed success[46, 47, 48].

Chapter 6

Conclusions and further work

The concept of beam-steering lens arrays has been developed in order to introduce automatic tracking to solar cookers. A fully functional small-scale prototype has been produced, and arguments have been made for the benefits of an up-scaled version of the concept. Before attempting to scale up the system, a number of challenges and potential developments should be addressed.

6.1 Further work

6.1.1 Improving lenslet geometry

In the optimization of the present prototype, a beam divergence of less than 2.5° degrees after the beam-steering lens array was specified, as described in Section 3.4.4. This was assumed to be sufficient for the application of solar cooking as argued in Chapter 2.2.6. Further work would involve investigating whether lens geometry could be improved using a stricter divergence requirement, or by having amount of divergence as part of the merit function and not just a requirement.

An 8 year old version of Zemax has been used for simulation and optimization. Further development should be done using newer versions of Zemax or related software, where some idiosyncrasies related to the age of the software might have been resolved[1]. Analytical design methods such as the Simultaneous Multiple Surface (SMS) method should also be investigated as an alternative to optimization. Such methods have benefits such as flexibility, speed and determinism.

[1]E.g.: Using global system folders for storing macros, apertures and display settings. Using the old DDE protocol for communication with external software. Low flexibility for customizing the behaviour of the built-in optimization routines. The use of an old and slow macro language that lacks basic functionality such as local variables, parameters and return values from subroutines. Storing different part of system state in different files.

6.1.2 Improving manufacturing process

The prototype beam-steering lens array introduces a divergence half-angle of $\approx 3.5°$ to the light, instead of the simulated $\approx 2°$ divergence half-angle. This is mainly due to the low surface quality as illustrated in Figure 4.9 on page 35. New manufacturing processes should be considered both for mold manufacturing and for lens molding in order to improve this quality.

6.1.3 Considering other materials

In the present project, PMMA was chosen as a material for the optical system. There is a trend within other solar energy systems of using PDMS optics instead of PMMA due to higher transmittance and better aging properties [41]. A more thorough comparison should therefore be performed to evaluate the choice of material.

6.1.4 Anti-reflective coating

Anti-reflective coatings have traditionally been difficult to apply to polymer optics due to problems such as high temperatures required in the coating process, poor adhesion, and so on. Recent developments, however, are increasing the performance and lowering the cost of such coatings for polymer optics [49, 50]. Applying such coatings to the lens arrays may offset the high Fresnel reflection losses at the optical surface. It may allow increasing the number of optical surfaces, which would increase system performance by enabling better control of optical aberrations.

6.1.5 Developing improved tracking algorithms

Improved and more robust tracking algorithms should be developed in order to ensure robust and accurate tracking, including changing sensor type from photocells to phototransistors. Required tracking accuracy and tracking forces should be estimated in order to choose appropriate actuators with good performance and as low price as possible. The feasibility of passive tracking as part of the lens arrays should also be investigated, as this would enable systems with even lower costs. Passive tracking might be implemented by using part of the incident energy to change system dimensions using bimetallic strips or related similar components.

6.1.6 Thorough optical design of a concentrator

The main focus of optical design in this thesis was the beam-steering lens array itself. In order to ensure optimum performance in a finished system, this should be coupled to thorough optical design of the optics in the concentrator, including a secondary reflector in order to increase concentration factors and homogenize flux density across the cooking surface.

6.1.7 Optimizing lenslet scale

The lenslets in the prototype have a diameter of 6.33mm. Being an afocal geometrical optical system, the arrays can be scaled up or down without affecting optical behaviour (until being scaled down to the order of the coherence length of sunlight). Scaling down the lens arrays will lead them to being thinner with less material usage, but it causes stricter tolerances and lower mechanical strength. A trade-off must therefore be made when choosing a lenslet scale.

6.1.8 Considering other applications

The concept of beam-steering lens arrays has a number of potential use-cases other than solar cooking, such as solar lighting, concentrator photovoltaics, or the control of beams from artificial light sources. These applications might have a higher commercial potential, so that it might be preferable to develop the concept for one of these applications first, in order to allow the technology to mature.

6.2 Conclusions

The feasibility of beam-steering lens array has been demonstrated for the application of solar cooking. The lens arrays can be made from common materials such as PMMA, and they can be compatible with high-volume production techniques such as injection molding or hot embossing. The additional divergence introduced by the lens arrays requires the use of concentrating optics with higher acceptance angle. This decreases the maximum achievable concentration ratio, but the achievable concentration factors are still high enough for applications such as solar cooking.

With increased incidence angle, intensity of sunlight received by a flat stationary receiver decreases due to the cosine projection effect. Even if the lens design is improved with a higher acceptance angle, full day cooking with no user involvement is impractical. The use of beam-steering lens arrays still significantly increases the user-friendliness of a direct solar cooker, by removing the need for continuous user involvement or complex mechanical systems in order to track the sun. Further development of this concept may therefore help increase solar cooker adoption across the world.

Bibliography

[1] *EA raises its five-year renewable growth forecast as 2015 marks record year*. URL: https://www.iea.org/newsroom/news/2016/october/iea-raises-its-five-year-renewable-growth-forecast-as-2015-marks-record-year.html (visited on 06/01/2017).

[2] *Google Scholar*. URL: https://scholar.google.no/ (visited on 05/31/2017).

[3] NTNU. *NTNU Open*. URL: https://brage.bibsys.no/xmlui/handle/11250/223328 (visited on 05/31/2017).

[4] *Advances in Solar Thermal Food Processing*. URL: http://www.consolfood.org/ (visited on 06/03/2017).

[5] John Twidell and Tony Weir. *Renewable Energy Resources*. English. 3 edition. London ; New York: Routledge, Jan. 2015. ISBN: 978-0-415-58438-8.

[6] *Solar Cookers International*. URL: http://www.solarcookers.org/ (visited on 05/31/2017).

[7] *Solar Cooker Distribution*. URL: http://www.solarcookers.org/our-work/solar-cooker-distribution/ (visited on 05/31/2017).

[8] Erdem Cuce and Pinar Mert Cuce. "A comprehensive review on solar cookers". In: *Applied Energy*. Special Issue on Advances in sustainable biofuel production and use - XIX International Symposium on Alcohol Fuels - ISAF 102 (Feb. 2013), pp. 1399–1421. ISSN: 0306-2619. DOI: 10.1016/j.apenergy.2012.09.002.

[9] N. L. Panwar, S. C. Kaushik, and Surendra Kothari. "State of the art of solar cooking: An overview". In: *Renewable and Sustainable Energy Reviews* 16.6 (Aug. 2012), pp. 3776–3785. ISSN: 1364-0321. DOI: 10.1016/j.rser.2012.03.026.

[10] Pia Piroschka Otte. "Solar cookers in developing countries—What is their key to success?" In: *Energy Policy* 63 (Dec. 2013), pp. 375–381. ISSN: 0301-4215. DOI: 10.1016/j.enpol.2013.08.075.

[11] Harry Apostoleris, Marco Stefancich, and Matteo Chiesa. "Tracking-integrated systems for concentrating photovoltaics". en. In: *Nature Energy* 1 (Mar. 2016), p. 16018. ISSN: 2058-7546. DOI: 10.1038/nenergy.2016.18.

[12] Jason H. Karp, Eric J. Tremblay, and Joseph E. Ford. "Planar micro-optic solar concentrator". EN. In: *Optics Express* 18.2 (Jan. 2010), pp. 1122–1133. ISSN: 1094-4087. DOI: 10.1364/OE.18.001122.

[13] Jason H. Karp et al. "Orthogonal and secondary concentration in planar micro-optic solar collectors". EN. In: *Optics Express* 19.104 (July 2011), A673–A685. ISSN: 1094-4087. DOI: 10.1364/OE.19.00A673.

[14] Ozgur Selimoglu and Rasit Turan. "Exploration of the horizontally staggered light guides for high concentration CPV applications". EN. In: *Optics Express* 20.17 (Aug. 2012), pp. 19137–19147. ISSN: 1094-4087. DOI: 10.1364/OE.20.019137.

[15] Hong-Yu Wu and Shu-Chun Chu. "Ray-leakage-free sawtooth-shaped planar light-guide solar concentrators". EN. In: *Optics Express* 21.17 (Aug. 2013), pp. 20073–20089. ISSN: 1094-4087. DOI: 10.1364/OE.21.020073.

[16] Justin M. Hallas et al. "Lateral translation micro-tracking of planar micro-optic solar concentrator". In: ed. by Lori E. Greene and Raed A. Sherif. Aug. 2010, p. 776904. DOI: 10.1117/12.860980.

[17] Panagiotis Kotsidas, Eleni Chatzi, and Vijay Modi. "Stationary nonimaging lenses for solar concentration". EN. In: *Applied Optics* 49.27 (Sept. 2010), pp. 5183–5191. ISSN: 1539-4522. DOI: 10.1364/AO.49.005183.

[18] Fabian Duerr, Youri Meuret, and Hugo Thienpont. "Tailored free-form optics with movement to integrate tracking in concentrating photovoltaics". EN. In: *Optics Express* 21.103 (May 2013), A401–A411. ISSN: 1094-4087. DOI: 10.1364/OE.21.00A401.

[19] Jared S. Price et al. "Wide-angle planar microtracking for quasi-static microcell concentrating photovoltaics". en. In: *Nature Communications* 6 (Feb. 2015), p. 6223. DOI: 10.1038/ncomms7223.

[20] Alex J. Grede, Jared S. Price, and Noel C. Giebink. "Fundamental and practical limits of planar tracking solar concentrators". EN. In: *Optics Express* 24.26 (Dec. 2016), A1635–A1646. ISSN: 1094-4087. DOI: 10.1364/OE.24.0A1635.

[21] Vinayak Narasimhan, Dongyue Jiang, and Sung-Yong Park. "Design and optical analyses of an arrayed microfluidic tunable prism panel for enhancing solar energy collection". In: *Applied Energy* 162 (Jan. 2016), pp. 450–459. ISSN: 0306-2619. DOI: 10.1016/j.apenergy.2015.10.051.

[22] Leo D. DiDomenico. "Towards doubling solar harvests using wide-angle, broadband microfluidic beam steering arrays". EN. In: *Optics Express* 23.24 (Nov. 2015), A1398–A1417. ISSN: 1094-4087. DOI: 10.1364/OE.23.0A1398.

[23] Noel León, Carlos Ramírez, and Héctor García. "Rotating Prism Array for Solar Tracking". In: *Energy Procedia*. 2013 ISES Solar World Congress 57 (2014), pp. 265–274. ISSN: 1876-6102. DOI: 10.1016/j.egypro.2014.10.031.

[24] Wang Lin, Pablo Benitez, and Juan Carlos Miñano. "Beam-steering array optics designs with the SMS method". In: vol. 8485. 2012, pp. 848505–848505–7. DOI: 10.1117/12.930759.

[25] Sergiy Valyukh, Iryna Valyukh, and Vladimir Chigrinov. "Liquid-Crystal Based Light Steering Optical Elements". en. In: *Photonics Letters of Poland* 3.2 (June 2011), pp. 88–90. ISSN: 2080-2242. DOI: 10.4302/photon.lett.pl.v3i2.210.

[26] R. Campbell and M. Machado. "LOW cost CPV = Embedded CPV with internal tracker". In: *2010 35th IEEE Photovoltaic Specialists Conference (PVSC)*. June 2010, pp. 003003–003007. DOI: 10.1109/PVSC.2010.5614802.

[27] *Eagle Rock Plastics — Mukwano Group*. URL: http://www.mukwano.com/brands/eagle-rock-plastics (visited on 05/31/2017).

[28] *Manufacturing — Mukwano Group*. URL: http://www.mukwano.com/division/manufacturing (visited on 05/31/2017).

[29] *One Earth Designs*. URL: https://www.kickstarter.com/profile/scotfrank (visited on 06/01/2017).

[30] *SOLGRILLEN 1,2X1,3M SVART OG SPEIL SOLSOURCE - Solgrill - Jernia.no*. URL: https://www.jernia.no/produktkatalog/hus-og-hage/griller/solgrill/solsource-solgrillen-1%2C2x1%2C3m-svart-og-speil-solsource/p/58013616 (visited on 06/01/2017).

[31] Per-Ivar Nikolaisen. *Softwarepioner og solgründer Jon "Sjeik Yahya" Bøhmer: Fra Amiga-eventyret Scala på en kyllinggård i Brumundal til hvordan lykkes som gründer i Afrika*. URL: http://shifter.no/index.php/2017/01/27/podcast-softwarepioner-solgrunder-jon-bohmer-amiga-pa-kyllinggard-brummundal-drommen-a-lykkes-mogadishu/ (visited on 06/01/2017).

[32] Katie Shanks, S. Senthilarasu, and Tapas K. Mallick. "Optics for concentrating photovoltaics: Trends, limits and opportunities for materials and design". In: *Renewable and Sustainable Energy Reviews* 60 (July 2016), pp. 394–407. ISSN: 1364-0321. DOI: 10.1016/j.rser.2016.01.089.

[33] Rajiv Laroia. *Inside the Development of Light, the Tiny Digital Camera That Outperforms DSLRs*. Oct. 2016. URL: http://spectrum.ieee.org/consumer-electronics/gadgets/inside-the-development-of-light-the-tiny-digital-camera-that-outperforms-dslrs (visited on 05/18/2017).

[34] Roland Winston et al. *Nonimaging Optics*. Saint Louis: Saint Louis : Elsevier Science, 2005. ISBN: 978-0-12-759751-5. URL: http://www.sciencedirect.com/science/article/pii/B9780127597515500014.

[35] Katherine Baker et al. "Practical implementation of a planar micro-optic solar concentrator". In: vol. 8485. 2012, pp. 848504–848504–6. DOI: 10.1117/12.929809.

[36] Edward A. Watson. "Analysis of beam steering with decentered microlens arrays". In: *Optical Engineering* 32.11 (1993), pp. 2665–2670. ISSN: 0091-3286. DOI: 10.1117/12.148100.

[37] Ata Akatay, Caglar Ataman, and Hakan Urey. "High-resolution beam steering using microlens arrays". EN. In: *Optics Letters* 31.19 (Oct. 2006), pp. 2861–2863. ISSN: 1539-4794. DOI: 10.1364/OL.31.002861.

[38] Jacques Duparré, Daniela Radtke, and Peter Dannberg. "Implementation of field lens arrays in beam-deflecting microlens array telescopes". EN. In: *Applied Optics* 43.25 (Sept. 2004), pp. 4854–4861. ISSN: 1539-4522. DOI: 10.1364/AO.43.004854.

[39] Soteris A. Kalogirou. *Solar Energy Engineering: Processes and Systems*. en. Google-Books-ID: wYRqAAAAQBAJ. Academic Press, Oct. 2013. ISBN: 978-0-12-397256-9. URL: http://www.sciencedirect.com/science/book/9780123745019.

[40] Julio Chaves. *Introduction to Nonimaging Optics, Second Edition*. en. Google-Books-ID: e11ECgAAQBAJ. CRC Press, Aug. 2015. ISBN: 978-1-4822-0674-6.

[41] David C. Miller and Sarah R. Kurtz. "Durability of Fresnel lenses: A review specific to the concentrating photovoltaic application". In: *Solar Energy Materials and Solar Cells*. Photovoltaics, Solar Energy Materials & Thin Films, IMRC 2009-Cancun 95.8 (Aug. 2011), pp. 2037–2068. ISSN: 0927-0248. DOI: 10.1016/j.solmat.2011.01.031.

[42] Zemax Development Corporation. *ZEMAX Optical Design Program User's Guide*. June 2009.

[43] David C. Lay. *Linear Algebra and Its Applications, Books a la Carte edition Plus NEW MyMathLab with Pearson eText – Access Card Package*. English. 4 edition. Place of publication not identified: Pearson, Dec. 2011. ISBN: 978-0-321-83614-4.

[44] Mikell P. Groover. *Principles of Modern Manufacturing: SI Version*. English. 4th International student edition edition. Hoboken, NJ: John Wiley & Sons Ltd, May 2010. ISBN: 978-0-470-50592-2.

[45] *How It Works — Morgan Solar*. URL: http://morgansolar.com/how-it-works/ (visited on 05/24/2017).

[46] Amos Veremachi et al. "PCM Heat Storage Charged with a Double-Reflector Solar System". en. In: *Journal of Solar Energy* 2016 (Aug. 2016), e9075349. ISSN: 2356-7635. DOI: 10.1155/2016/9075349.

[47] Ragnhild Skahjem and Silje Fosseng Duley. "Oil Based Solar Concentrator with Heat Storage". eng. In: *176* (2016). URL: https://brage.bibsys.no/xmlui/handle/11250/2405585 (visited on 12/23/2016).

[48] Asfafaw Haileselassie Tesfay. *Experimental Investigation of a Concentrating Solar Fryer with Heat Storage*. eng. NTNU, 2015. ISBN: 978-82-326-0780-8. URL: https://brage.bibsys.no/xmlui/handle/11250/281376 (visited on 12/23/2016).

[49] Chia-Jen Ting et al. "Low cost fabrication of the large-area anti-reflection films from polymer by nanoimprint/hot-embossing technology". en. In: *Nanotechnology* 19.20 (2008), p. 205301. ISSN: 0957-4484. DOI: 10.1088/0957-4484/19/20/205301.

[50] Baomin Wang, Jared S. Price, and Noel C. Giebink. "Durable broadband ultralow index fluoropolymer antireflection coatings for plastic optics". EN. In: *Optica* 4.2 (Feb. 2017), pp. 239–242. ISSN: 2334-2536. DOI: 10.1364/OPTICA.4.000239.

Appendix A

Paper on beam-steering lens array

Lateral translation beam-steering lens array for solar thermal energy applications

Håkon J. Dugstad Johnsen

June 11, 2017

Abstract

Concentrated solar thermal energy systems can achieve significantly higher energy efficiency than solar photovoltaic systems, but their utilization is complicated by the need to accurately rotate the whole concentrator optic in order to track the apparent motion of the sun. In this work, we propose the use of beam-steering lens arrays for solar tracking, and demonstrate a design that can track sunlight with a simulated $\approx$ 70% efficiency across $\pm 40^\circ$ tracking range, using millimeter-scale lateral translation and introducing less than $\pm 2^\circ$ divergence to the beam. The lens arrays are compatible with high-volume production techniques such as injection molding. The $\pm 40^\circ$ tracking range can be used to achieve 5.3h stationary operation, or full day operation with simple external tracking. By eliminating the need to rotate the concentrator element for solar tracking, this technology may enable the production of low-cost and robust small-scale consentrated solar thermal energy systems, facilitating the adoption of such systems across the world. The technology may also be used for other solar energy applications such as CPV systems, and solar lighting systems.

The design is simulated and optimized in Zemax OpticsStudio, and a fully functional prototype has been manufactured by compression molding of PMMA. The prototype demonstrates $\approx$60% efficiency and introduces $\pm 4^\circ$ divergence to the beam. With improved production techniques, the performance is expected to approach the simulated values.

1 Introduction

In recent years, solar energy usage has increased rapidly with the advent of low-cost PV technology. For thermal energy applications, concentrated solar thermal energy systems can provide significantly higher efficiency than PV systems, but this requires accurate tracking of the apparent motion of the sun. In large-scale heliostat systems, tracking is accomplished by rotating many small individually controlled mirrors, but this is impractical for small-scale systems. Instead, the entire optical assembly is usually rotated to be kept normal to the sun, and this introduces several complicating factors such as wind loads, the challange of balancing the center of mass, impractical location of the absorber and so on. Recently, several new concepts for solar tracking have been proposed, especially in the field of concentrator photovoltaics [1, 2, 3].

This work proposes the use of beam-steering lens arrays which can be placed in front of conventional concentrator optics as illustrated in Figure 1. By combining this with conventional concentrating optics, concentrated solar energy can be provided over 5 hours without reorienting the system.

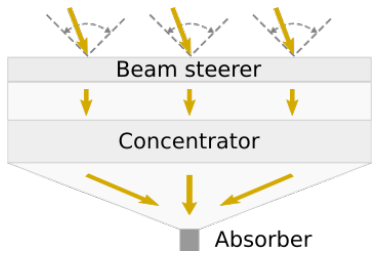

Figure 1: *Conceptual sketch of how a beam-steering lens array can be combined with conventional concentrating optics.*

2 Beam-steering lens arrays

Beam-steering lens arrays have previously been proposed for steering of laser beams [4, 5] and also recently for solar energy and steerable LED lighting applications [3]. For laser beam-steering, a beam-steering lens array receives a beam parallel to its optical axis and emits it at an angle. For solar energy applications, the beam-steering lens array must be operated in reverse, receiving a beam at an angle, and emitting it parallel to the optical axis, as shown in Figure 2a.

In this work, a keplerian type type beam-steering device is described. Within the limits of the paraxial domain, such a device consists of two thin lenses separated by their total focal lengths $f_1 + f_2$ as illustrated in Figure 2a. Such a system can track incoming sunlight at an angle θ by translating the last lens array a distance Δx:

$$\Delta x = f_1 \cdot \tan\theta \tag{1}$$

In order for all rays to reach the correct lens in the array L_2, the second focal length must be smaller than the first, giving an angular magnification factor M:

$$M = \frac{f_1}{f_2} = 1 + \frac{N}{2}\tan\theta_{max} \tag{2}$$

Sunlight has an inherent divergence of $\pm 0.27°$ [6, p. 49]. In order to allow high concentration optics behind the beam-steering lens array, it is desirable that the angular magnification of the system is low. By adding a field lens L_f to the system, as shown in Figure 2b, identical focal lengths f and an angular magnification of unity can be achieved[4].

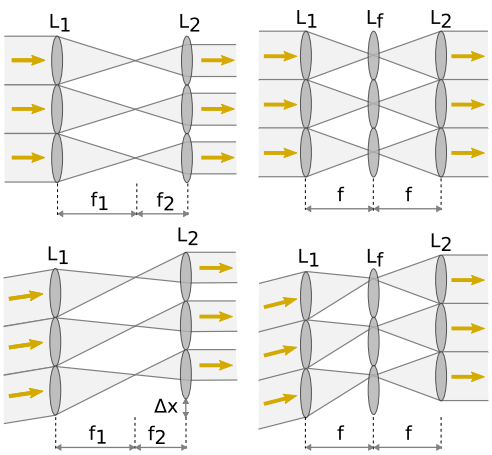

(a) *Keplerian beam-steering principle, using back-to-back lenses with different focal lengths.*

(b) *Keplerian beam-steering principle including field lens and lenses with equal focal lengths.*

Figure 2

2.1 Designing a practical beam-steering lens array

In order to implement a beam-steering design with high efficiency over a large field of view, some modifications must be done to the basic principles in Figure 2a and Figure 2b:

- With Fresnel reflection losses of approximately 4% per optical surface, it is desireable to avoid the two extra surfaces of the field lens in Figure 2b. Therefore, lens array L_1 is instead made thicker so that its second surface partially fulfills the purpose of a field lens.
- For wide field of view, field curvature becomes significant, and purely planar tracking is not sufficient.
- The wide field of view and wide lenses operate outside the paraxial domain, and large aberrations are introduced. In traditional lens design, aberrations are reduced by introducing additional optical surfaces and using apertures that are smaller than the system diameter. Due to the close packing in a lens array, no lens can be wider than the system aperture, and for efficiency reasons, additional surfaces can not be added. Aspheric surfaces must therefore be used to compensate for the aberrations.

A three-dimensional model of the beam steerer was created and optimized using a legacy version of Zemax OpticsStudio. Translation of the second lens array as a function of input angles is implemented using Zemax multi-configuration functionality. With many aspheric terms for each surface, there is a large number of optimization variables. In order to improve optimization performance, a multilevel optimization strategy has been implemented as illustrated in Figure 3a. For each iteration of the outer optimization loop, the inner loop calculates the optimal shape of the final surface. Figure 3b illustrates which parameters are optimized in the inner optimization loop (green) and which parameters are optimzied in the outer optimization loop (red). The inner optimization loop is similar to the concept of a direct "Solve" in Zemax [7, p. 447], in which the curvature or thickness of one surface is automatically adjusted to bring the system into focus, but the built-in Zemax functionality only handles the paraxial performance of the system. In the present system with large angles, wide aspheric surfaces and multiple configurations, the built-in "Solve" in Zemax is not sufficient.

The inner optimization solution is implemented as a Zemax-script in ZPL (Zemax Programming Language). A number of rays are traced up to the final surface for a number of incoming solar angles. When the rays reach the final surface, the required surface inclination at that exact point is solved using Snell's law. Polynomial terms describing an optimal surface are solved using a direct linear least squares method.

The updated surface shape slightly changes the ray's point of intersection with the surface, so the process is iterated a few times until convergence.

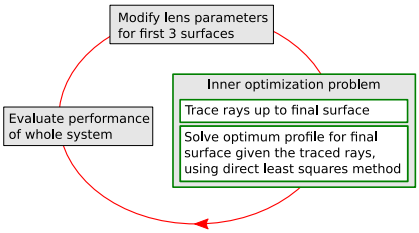

(a) *Diagram of the implemented optimizaton procedure.*

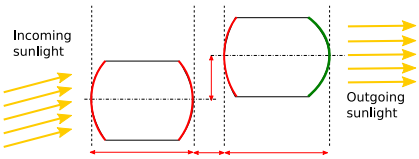

(b) *Overview of the variables that are being optimized. The red surfaces and dimensions are part of the outer optimization problem. The green surface is solved directly in the inner optimization problem.*

Figure 3

2.2 Optimization results

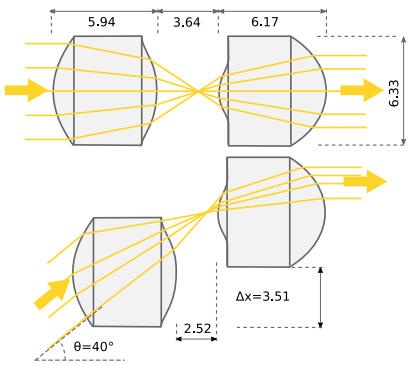

Figure 4: *Final geometry of lens arrays, here shown for input angles of 0° and 40°. All length units are millimeters.*

A beam-steering lens array is optimized in using the optimization routines in Zemax combined with the previously described multilevel optimization strategy. The system is optimized over ±40° range, with a permitted divergence after the beam-steering lens array of ±2.5°. Lens material is PMMA, and the system is evaluated using an approximation of the AM1.5D spectrum across the spectral range for which the PMMA data is available in the Zemax Glass Catalog. Tracking is restricted to a spherical path, in order to simplify the kinematics of the structure that will hold the lens arrays.

The resulting lens geometry is shown in Figure 4. The individual lenslets have a hexagonal aperture, for close packing in a lens array. The simulted performance of the resulting beam-steering lens array across its field of view is shown in Figure 7. The divergence half-angle after the lens arrays is $\leq 2°$. Although this is significantly higher than the inherent 0.27° divergence half-angle of sunlight, it is still high enough to achieve notable concentration factors. Maximum possible concentration ratio after the lens array is $C_{max} = 821$, while maximum concentration ratio for a more practical NA = 0.5 concentrating optics is $C_{max,NA=0.5} = 205$.

$$C_{max} = \frac{1}{(\sin(2°))^2} = 821 \quad (3)$$

$$C_{max,NA=0.5} = \frac{0.5^2}{(\sin(2°))^2} = 205 \quad (4)$$

2.3 Field curvature and kinematics

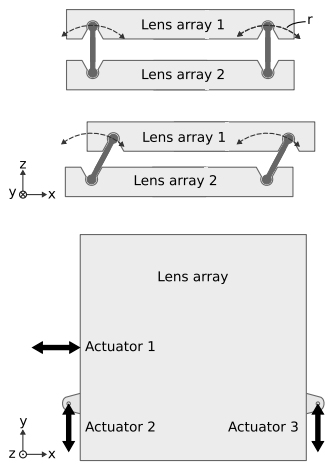

Figure 5: *Illustration of links and actuators that can be used to control the relative movement of the lens arrays.*

In a complete system, the two lens arrays must be attached to a mechanical system that supports translation along the x and y axes, while also controlling the separation along the z axis in order to follow the

field curvature. This can be implemented by connecting the two lens arrays using links whose radius is the inverse of the field curvature as illustrated in Figure 5. This also prevents rotation about the x and y axes. Translation along the x and y axes as well as rotation about the z axis can be controlled using three external actuators.

3 Prototype

A functional prototype with automatic tracking has been created using the lens design from Section 2.2. As an example use case, the system is attached to an off-axis parabolic reflector that illuminates a target from the underside. This specific configuration is a scaled-down version of a solar cooking concept using beam-steering lens arrays.

As can be seen from the 3D model in Figure 6a, this model only uses two actuators in the form of micro servos. The final degree of freedom is instead controlled kinematically by connecting the rotation of the individual links that connect the two lens arrays. Experience from this prototype shows that it is difficult to meet the tolerance requirements for rotation about the z axis in this configuration, and that it would be better to use a third actuator.

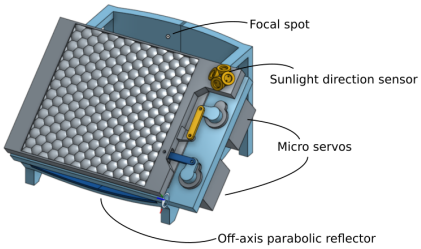

(a) *Proof of concept 3D model*

(b) *Proof of concept with integrated automatic tracking tested outside in the sun*

Figure 6

3.1 Methods

Molds for the lens arrays were machined in aluminum on a milling machine. These molds were used for compression molding of PMMA plates.

The tracking motion is actuated using SG-92R micro servos and controlled from an Arduino Nano development board. The system uses a combination of open- and closed-loop control, and both control loops have been implemented with low-cost photocells: Approximate solar position is detected using a set of four inclined photocells, each inclined $\pm 40°$ from the front plane about its respective axis, and the microcontroller orients the array to this approximate position. Secondly, a small section of the input aperture is diverted to a set of photocells that measure tracking error, and a closed loop control loop is implemented in order to minimize this tracking error.

3.2 Results

Performance of the beam-steering lens array prototype has been measured using image analysis, as shown in Figure 7. The results show $\approx 10\%$ reduced efficiency compared to the simulated values, and a $\approx 75\%$ increase of divergence compared to simulation. This is also visible in the encircled energy plots shown in Figure 8. The high divergence is likely a result of a waviness in the surface of the lens array, which is an artifact of the mold manufacturing process. With improved mold manufacturing and corresponding increased surface quality, future prototypes are expected to better follow the predicted performance.

4 Discussion

We have shown that beam-steering lens arrays can be used to track and redirect sunlight with low losses over a $\pm 40°$ incident range. Lens arrays can be made from common materials such as PMMA, and they can be compatible with high-volume production techniques such as injection molding or hot embossing. This can facilitate a number of solar energy applications including solar cooking, small-scale solar thermal processing, solar water heating, concentrator photovoltaics and solar lighting. The small range of motion and the low inertia of the lens arrays allows greatly increased tracking speed, which could enable tracking on moving platforms such as boats and vehicles. The small tracking motions may also enable the development of integrated passive tracking systems,

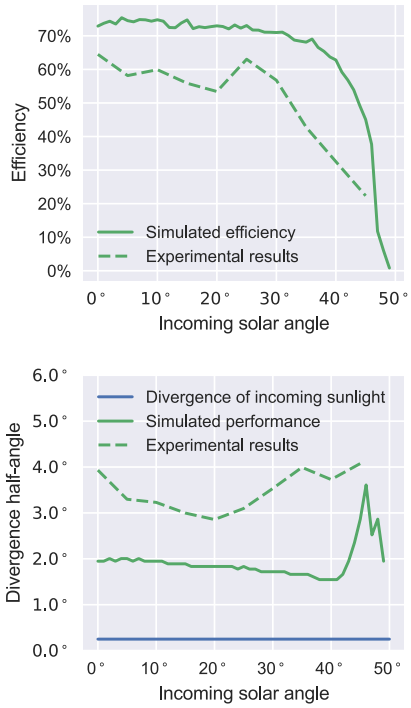

Figure 7: *Simulated and measured efficiency and divergence of the prototype over its field of view. Divergence half-angle has been defined as the angle at which the beam intensity has reached 10% of maximum intensity.*

further lowering the cost of automatic tracking.

The additional divergence introduced by the lens array requires the use of concentrating optics with higher acceptance angle, decreasing the maximum achievable concentration ratio. The achievable concentration ratios are still high enough for many applications, and future improvements in the design of the lenses might decrease the divergence. Recent applications in the application of anti-reflective coatings on polymer optics[8, 9] may increase the practicality of the concept by increasing efficiency and enabling the use of more optical surfaces to control optical aberrations.

With increased incidence angle, intensity of sunlight received by a flat stationary receiver decreases due to the cosine projection effect. Even if the lens design is improved with a higher acceptance angle, efficiency will therefore be low for high incidence angles, and some amount of external tracking might be required for efficient full-day operation. The use of beam-steering lens arrays still significantly reduces the requirements for this external tracking, and may therefore foster the development of low-cost, small-scale, robust and maintainable solar thermal energy systems.

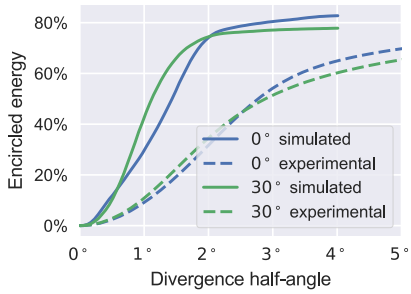

Figure 8: *Measured and simulated encircled energy for prototype, with 0° and 30° incident sunlight. The encircled energy is scaled against total solar energy incident on the beam-steering lens array. Polarization dependent Fresnel reflection losses are considered, cosine projection loss is not.*

References

[1] Harry Apostoleris, Marco Stefancich, and Matteo Chiesa. "Tracking-integrated systems for concentrating photovoltaics". en. In: *Nature Energy* 1 (Mar. 2016), p. 16018. ISSN: 2058-7546. DOI: 10.1038/nenergy.2016.18.

[2] Alex J. Grede, Jared S. Price, and Noel C. Giebink. "Fundamental and practical limits of planar tracking solar concentrators". EN. In: *Optics Express* 24.26 (Dec. 2016), A1635–A1646. ISSN: 1094-4087. DOI: 10.1364/OE.24.0A1635.

[3] Wang Lin, Pablo Benitez, and Juan Carlos Miñano. "Beam-steering array optics designs with the SMS method". In: vol. 8485. 2012, pp. 848505–848505–7. DOI: 10.1117/12.930759.

[4] Edward A. Watson. "Analysis of beam steering with decentered microlens arrays". In: *Optical Engineering* 32.11 (1993), pp. 2665–2670. ISSN: 0091-3286. DOI: 10.1117/12.148100.

[5] Ata Akatay, Caglar Ataman, and Hakan Urey. "High-resolution beam steering using microlens arrays". EN. In: *Optics Letters* 31.19 (Oct. 2006),

pp. 2861–2863. ISSN: 1539-4794. DOI: 10.1364/OL.31.002861.

[6] Soteris A. Kalogirou. *Solar Energy Engineering: Processes and Systems*. en. Google-Books-ID: wYRqAAAAQBAJ. Academic Press, Oct. 2013. ISBN: 978-0-12-397256-9. URL: http://www.sciencedirect.com/science/book/9780123745019.

[7] Zemax Development Corporation. *ZEMAX Optical Design Program User's Guide*. June 2009.

[8] Chia-Jen Ting et al. "Low cost fabrication of the large-area anti-reflection films from polymer by nanoimprint/hot-embossing technology". en. In: *Nanotechnology* 19.20 (2008), p. 205301. ISSN: 0957-4484. DOI: 10.1088/0957-4484/19/20/205301.

[9] Baomin Wang, Jared S. Price, and Noel C. Giebink. "Durable broadband ultralow index fluoropolymer antireflection coatings for plastic optics". EN. In: *Optica* 4.2 (Feb. 2017), pp. 239–242. ISSN: 2334-2536. DOI: 10.1364/OPTICA.4.000239.

Appendix B

Abstract submitted to CONSOLFOOD Conference 2018

The following abstract has been submitted to the CONSOLFOOD Conference 2018. Note on system efficiency: The abstract quotes a total system efficiency of $\approx 30\%$ for the prototype, which was measured within a $8\mathrm{mm}$ radius target area using image analysis. After submitting the abstract, it was discovered that the correct radius of the scaled-down target area was in fact $5.9\mathrm{mm}$ as described in Section 4.4.7 of the main thesis. This leads to a total system efficiency closer to $\approx 20\%$, as shown in Figure 4.17 of the main thesis, but measurement uncertainties are high..

BEAM STEERING LENS ARRAY FOR SOLAR COOKING

Håkon J. D. Johnsen[1] *, Ole Jørgen Nydal[2], Jan Torgersen[1]

1: Department of Mechanical and Industrial Engineering, Norwegian University of Science and Technology,
NTNU, NO-7491 Trondheim, Norway
e-mail: hakon.d.johnsen@gmail.com, jan.torgersen@ntnu.no, web: http://www.ntnu.edu
2: Department of Energy and Process Engineering, Norwegian University of Science and Technology
e-mail: ole.j.nydal@ntnu.no

Abstract: Operation of concentrator based solar cookers is complicated by the need to accurately rotate the large parabolic mirror for solar tracking. Here we demonstrate a workaround. Via beam steering lens arrays, we can track sunlight with a simulated >70% efficiency across ±35° tracking range, using millimeter-scale lateral translation. This eliminates the need to rotate the mirror, facilitating the design of a simpler cooker. Full-day cooking can be achieved by manually reorienting the cooker 1-2 times a day in the general direction of the sun, while accurate automated tracking is performed by small low-cost actuators. Additional features such as adjustable power level can also be implemented.

The optical system was simulated and optimized using Zemax OpticStudio, and a functional 1:15 scale prototype has been constructed. The prototype demonstrates a promising total system efficiency of ≈30%, which is expected to rise to 50%-60% with improved manufacturing of the array. The lens array is assumed to be compatible with injection molding, enabling low-cost high-volume production. By enabling low-cost automatic tracking, this technology may facilitate inexpensive, maintainable and user-friendly solar cooking, fostering its increased adoption across the world.

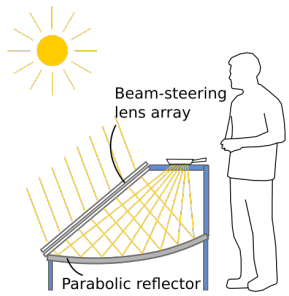

Figure 1: Sketch of solar cooking concept using beam steering

Figure 2: Functional small prototype with automatic tracking.

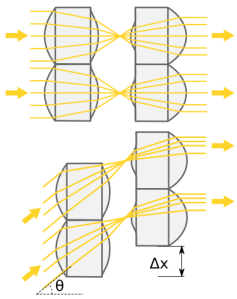

Figure 3: Illustration of how lateral translation of a lens array Δx can redirect sunlight arriving at an angle θ

Keywords: Solar cooking, Beam steering, Automated tracking, Lateral translation

Appendix C

Parabolic features in Onshape

Most of the 3D modelling in this project has been done in Onshape, a parasolid-based parametrical mechanical CAD software system running in the cloud [1]. At the beginning of this project, Onshape did not have native support for conical curves. In order to simplify the modelling, an extension was written using the Onshape programming language Featurescript [2], in order to easily generate 3D models with parabolic surfaces.

The extension takes a focus point, an aperture, a point on the surface to be created and a thickness. From this, it generates a solid body whose inner surface has a parabolic shape with the given parameters. The parabolic surface is created by generating an array of 3D points that describe the surface, based on the corresponding quadratic polynomial. This array of points is used to generate 3D splines, which are used as guides for a Loft feature[3] that generates the surface. The complete source code is included as an attachment with the name ParabolicShape.txt. The feature is also available online at ParabolicShape (link in digital copy of the thesis) and can be used by any Onshape user.

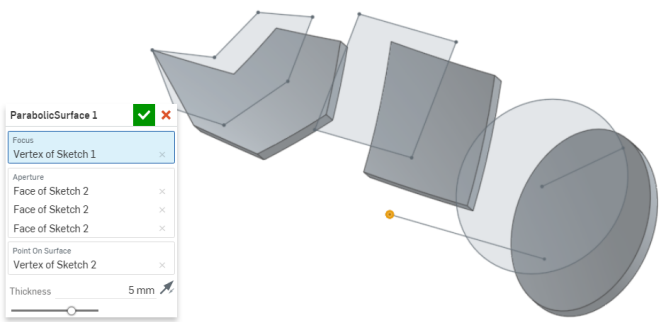

Figure C.1: Demonstration of parabolic feature extension to Onshape, here shown to work with multiple different apertures.

References for Parabolic surface generator in Onshape

[1] Onshape. *FAQs — Onshape*. URL: https://www.onshape.com/faqs (visited on 05/24/2017).

[2] Onshape. *FeatureScript — Onshape*. URL: https://www.onshape.com/featurescript (visited on 05/24/2017).

[3] *Loft*. URL: https://cad.onshape.com/help/Content/loft.htm (visited on 05/24/2017).

Appendix D

Justification for the use of image analysis

Due to the wide scope of this project, there was not enough time at the end of the project to acquire and use professional optical equipment for estimating efficiency of the prototypes. In order to still get some useful efficiency data despite the lack of such equipment, a provisional test-rig was constructed from 3D printed and off the shelf components, and performance measurements were performed using image analysis. Image analysis was performed on images from the consumer-grade digital system camera Olympus Pen E-P1. This image analysis depends on a number of assumptions, which are justified in this appendix:

- The image sensor is linear with respect to radiant intensity of the surface being imaged.
- Lens vignetting is negligible.
- The results are generalizable to the full solar spectrum.
- The reflectance of white office paper is diffuse and approximately lambertian.
- The accuracy of the relative positions of the optical components is acceptable despite low precision.

D.1 Linearity of the image sensor

The CMOS image sensor of a digital camera is considered a linear device. The brightness values stored in a regular JPEG image file are unsuitable for scientific image analysis due to the number of transformations that are applied to the values from the image sensor, including gamma transformation, white balance correction, contrast adjustments, possibly tone-mapping and so on. However, by reading the raw sensor values directly, the values

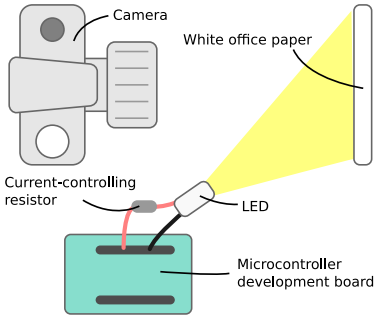

(a) Test setup.

(b) Resulting photos with increasing brightness.

Figure D.1: Testing the linearity of the image sensor.

are expected to be much more linear with respect to radiance. In order to verify this, the following test was carried out using the test setup illustrated in Figure D.1a:

- An Arduino microcontroller development board controls a LED, whose normalized radiant intensity can be precisely controlled using pulse-width modulation.
- The LED illuminates a white office paper.
- A camera is pointed towards this office paper.
- The camera is configured with fixed exposure settings (f/5.6, ISO200, exposure 1/8s) and raw file format.
- A set of pictures are taken under different levels of illumination from the LED.

The resulting images are shown in Figure D.1b. These raw images are imported into Python [1], using rawpy [2], where the raw values from the sensor can be analyzed. The average sensor value for each color channel and plotted against the corresponding radiant intensity of the LED. The resulting data can be seen in Figure D.2, where a best-fit linear line is plotted against the data. This demonstrates that the linearity of the image sensor is

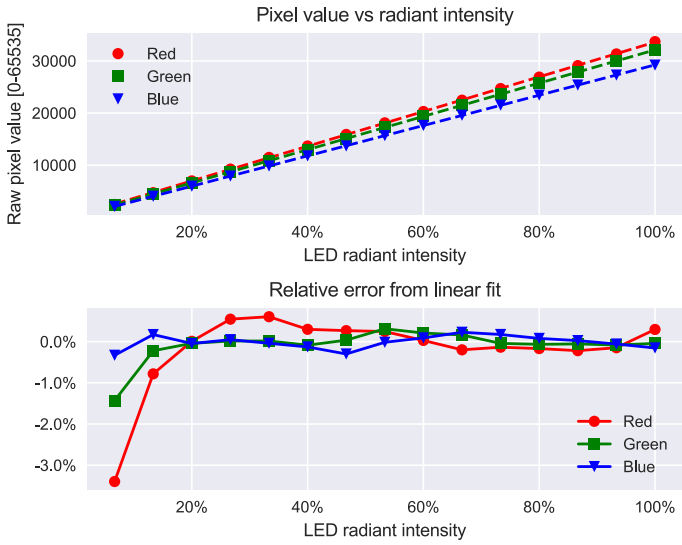

Figure D.2: Results from testing linearity of the image sensor using the test setup in Figure D.1a.

very good, with an error of less than $\pm 0.5\%$ except at the very lowest end of the dynamic range of the sensor.

D.2 Vignetting

Vignetting is the gradual decline of image brightness towards the edges of the field of view, due to a number of different factors. This can lead to inconsistent results when comparing brightness values from different parts of the image. In order to measure the amount of vignetting in the camera, photos were shot of an evenly illuminated sheet of paper as illustrated in Figure D.3. The paper is evenly illuminated because the distance to the light source is approximately constant ($L \gg \Delta L$ as shown in the figure). Assuming that the paper reflects light diffusely, the radiation intensity from the paper is independent of direction, [3, p. 696] and the camera should observe a constant brightness across the piece of paper.

Results from the test can be seen in Figure D.4 for different lens configurations. It can be seen that vignetting is fairly strong for all configurations, and stopping down the lens does not significantly reduce amount of vignetting. In order to circumvent this vignetting, image analysis is done using cropped images. By cropping the image to the centermost 1000px by 1000px, there is less than 10% difference between the center of the image and its edges, as can be seen in Figure D.5.

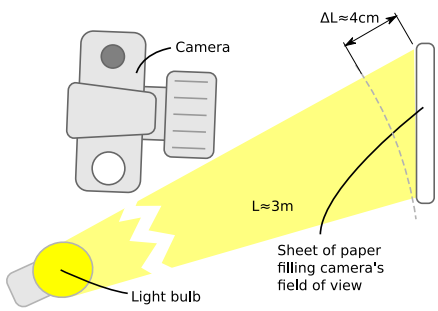

Figure D.3: Test setup for measuring vignetting.

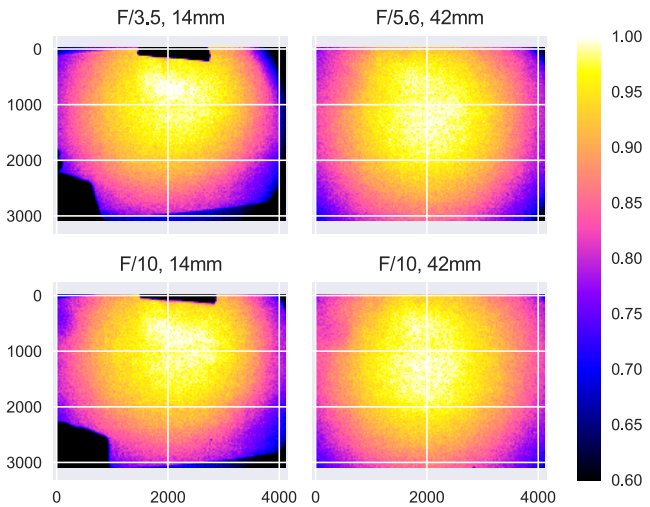

Figure D.4: Normalized brightness values across the camera's field of view when shooting a picture of an evenly illuminated sheet of paper. Values are averaged across the red, green and blue channel.

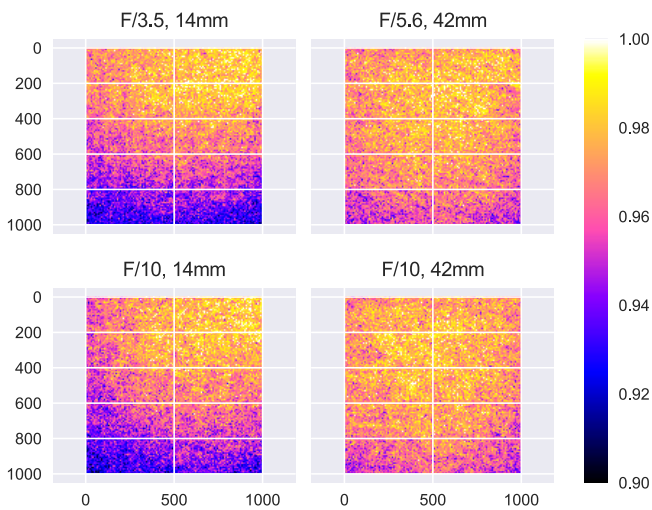

Figure D.5: Normalized brightness across a cropped field of view.

D.3 Solar spectrum

Using image analysis, lens array efficiency can be measured across the visible spectrum using the red (˜650nm), green (˜550nm) and blue (˜450nm) channels of the camera. Solar radiation, on the other hand, is spread over wavelengths between $300\mathrm{nm}$ to $2500\mathrm{nm}$ [3, p. 709]. According to the AM1.5D model, approximately 45% of solar energy falls within the visible range of 400nm-700nm[4]. Because of this, the measured efficiency is not a complete measurement of system efficiency, but only a measurement for those specific wavelengths.

There are two main factors that can affect the performance of the beam-steering lens array for different wavelengths:

- Absorption bands in the material. PMMA has fairly good transmittance across the solar spectrum. PMMA has some strong absorbtion bands at approximately $1600\mathrm{nm}$ and higher that might affect performance to some degree, but the total effect is assumed small due to the low solar intensities at these wavelengths.

- Different refractive index for different wavelengths, causing dispersion. This might be a significant factor, in a system where other losses are controlled. In the current prototypes, however, no noticeable performance differences are detected between the different channels on the camera. Because of this, it is assumed that for the current prototypes, the effect of dispersion is insignificant compared to divergence caused by low surface quality.

For the completed system,integrated efficiency across the full solar spectrum can be measured by measuring rate of temperature rise of a known quantity of water placed in the focal spot, compared to known solar irradiance at that point in time. Such measurements have been performed, as reported in Section 4.4.7.3, but the solar intensity measurements at NTNU are out of order, so it was not possible to compare the values to known irradiance.

D.4 Accuracy of camera exposure settings

When comparing focused and unfocused light in order to evaluate performance of the lens array, the dynamic intensity range is so large that the measurements can not be performed using constant exposure settings on the camera. With constant exposure settings, either the focused light would be over-exposed or the unfocused light would be under-exposed.

There are 3 exposure settings on a digital camera camera that control the values in the resulting RAW file:

- Exposure time: Measured intensity increases linearly with increased exposure time.

- F-number: Controls the aperture size of the lens. Measured intensity is inversely proportional to the square of the f-number.

- ISO setting: Controls the gain on the ADC that reads the pixel values. Measured intensity increases linearly with ISO value.

By reading the image metadata, the captured values can therefore be correlated between different exposure settings, and intensity can be compared across a larger dynamic range. An exposure-independtent intensity value I can be calculated using the following equation, where P is the raw pixel value, F is f-number, E is exposure time and ISO is the ISO-setting

$$I = \frac{P \cdot F^2}{E \cdot ISO} \tag{D.1}$$

This was tested using the same test setup as the test setup for linearity in Section D.1 on page 75, but the camera was configured for automatic exposure settings. The results are shown in Figure D.6 on the next page. As can be seen, there is a linear trend, but there is significant amount of noise, with relative errors of approximately $\pm 15\%$. It is believed that the large error is due to the mechanical nature of the aperture setting and the exposure time setting (the camera has a mechanical shutter). The ISO setting, however, is a purely electronic gain on the ADC, and is believed to be more predictable. A new test was therefore performed, limiting the camera to only changing ISO setting, and not the other exposure settings, the linearity error is now reduced to approximately $\pm 2\%$ except at very low intensity values.

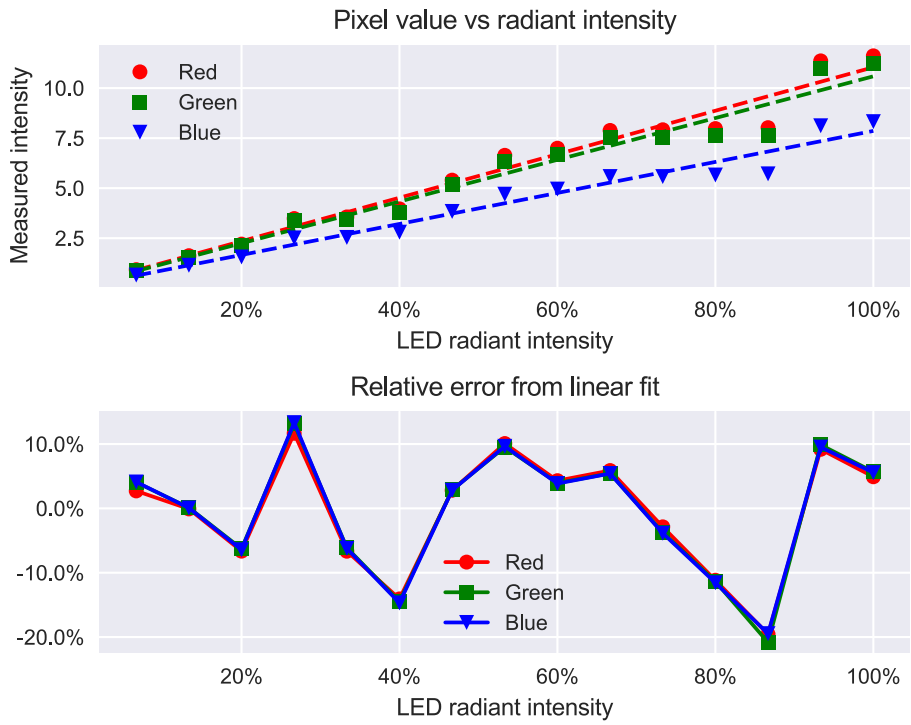

Figure D.6: Measured linearity of measurements using Equation D.1 on the previous page to correlate values across different exposure settings in the camera.

Figure D.7: Measured linearity of measurements using Equation D.1 on page 81 to correlate values across different exposure settings in the camera. Higher linearity is achieved by only varying ISO setting, not aperture or exposure time.

D.5 Test setup for beam-steering lens arrays

The relevant performance indicators for the bare beam-steering lens arrays are:

- Transmission efficiency.
- Beam divergence after lens array.

These performance indicators are measured using the test setup shown in Figure D.8

The LED is driven with a constant, controlled current. The LED has a square die with a size of approximately $1.4\text{mm} \cdot 1.4\text{mm}$. When collimated at a 155mm focal length, this gives a divergence half-angle of $\phi = \frac{0.7\text{mm}}{155\text{mm}} \cdot \frac{180^\circ}{\pi} \approx 0.26^\circ$ which is comparable to the divergence of sunlight. Lenses L_1 and L_2 are low-quality glass lenses with spherical surfaces and $f_1 = f_2 = 155\text{mm}$ focal lengths. In order to limit spherical and chromatic aberration from the test setup, a relatively narrow aperture diameter $A_1 = 20\text{mm}$ is used.

A 3D printed spacer is used for accurately adjusting the incoming angle θ with 5° increments. For each angle, the lens arrays are adjusted manually, a and a photo is shot using the camera.

By analizing the size of the spot on the image surface, beam divergence after the lens array can be analyzed. Corresponding efficiency is measured by comparing this to the total amount of light in the system when the lens array is removed. An example of a raw dataset is shown in Figure D.9. The numbered images represent an incoming angle θ, and are photos of the image surface when the beam-steering lens array is used to redirect light coming from this angle. The image named Spot.ORF is an image of the system when $\theta = 0^\circ$ and the beam-steering lens array is removed. The image named Spot_defocus.ORF is similar to Spot.ORF, but lens array L_2 is moved further away from the image surface. This leads to a defocused spot with the same amount of energy but a lower maximum intensity. This defocused spot is used as a reference for the available amount of energy

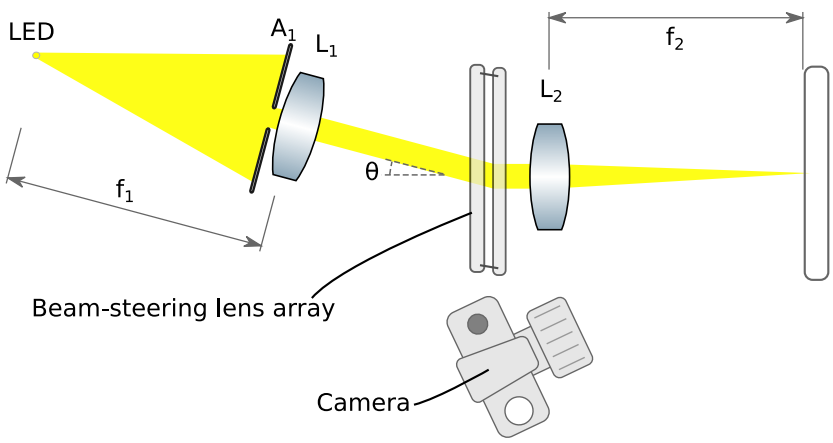

Figure D.8: Test setup for testing the lens array. Light from the LED is collimated using lens L_1, and redirected using the beam-steering lens array. The divergence of the resulting beam is imaged onto the image surface using lens L_2, and the camera is used for analyzing this image.

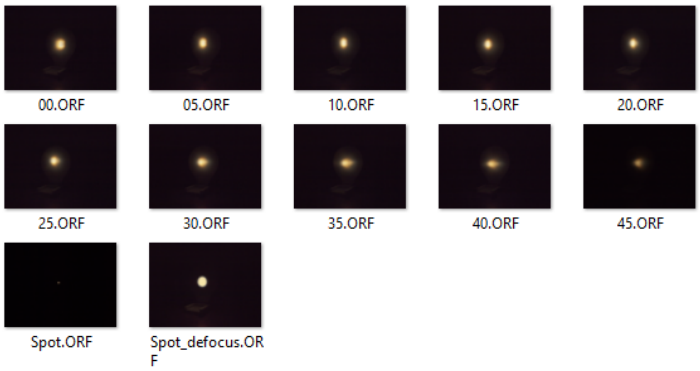

Figure D.9: Example of a raw dataset from testing beam-steering lens array performance.

because it can be shot at the same exposure settings as the other measurements.. Example plots of beam divergence is displayed in Figure D.10.

The images are analyzed using Python, and the results are shown in Figure 4.17 of the main thesis. The Python together with all generated plots is included in the 'Python'-folder in the attachments to this thesis.

D.5.1 Measurement accuracy

All the analyzed photos are shot using the same exposure settings, and sensor values are around the middle of the sensor's dynamic range. This means that the accuracy of the intensity measurements are expected to lie within the $\pm 0.5\%$ uncertainty that was measured in Section D.1 on page 75. The manual tracking of the array may introduce significant uncertainties. In order to limit the consequences of incorrect manual tracking, the Python code automatically detects the center of the redirected spot, even if it is slightly offset from parallel to the optical system. Calibration of system dimensions has been done with approximately 1% uncertainty using photos of a ruler placed at the image surface. Focal length is also known to approximately 1% uncertainty.

Measurements are therefore expected to be within an uncertainty of approximately $\sqrt{0.01^2 + 0.005^2 + 0.01^2} \approx 1.5\%$, and this test is expected to give a very good indication of system performance for visible light.

D.5.2 Cosine projection loss

An important factor to consider for stationary solar collectors is the cosine projection loss: When incident angle increases, the same sunlight is spread over a larger area of the stationary receiver, decreasing in intensity with the cosine of the incident angle. The test setup shown in Figure D.8 uses only a fraction of the surface of the lens arrays, so the entire beam is redirected despite arriving at lower intensity over a larger area of the lens arrays. This leads to efficiency measurements that ignore the cosine projection loss. In real conditions, the entire lens array receives sunlight, so decreased intensity causes decreased

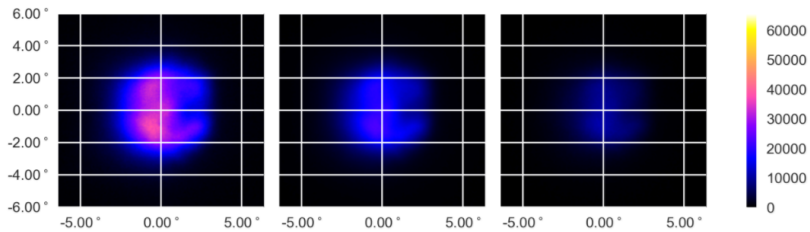

(a)

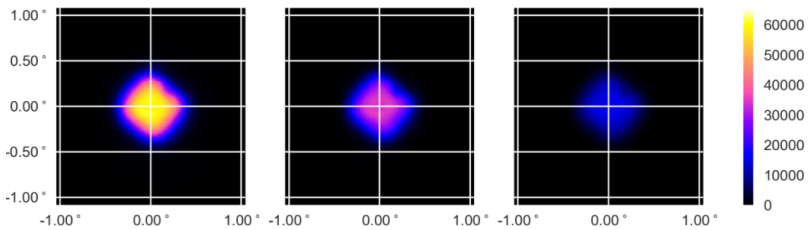

(b)

Figure D.10: Plots of angular composition of beam divergence at 0° incident angle. With (a) and without (b) beam-steering lens array. The displayed intensity values are the raw unprocessed values from the camera (0-65535), and the three plots represent the red, green and blue channel of the camera.

apparent efficiency of the system. At maximum incident angle for the present system of $\theta = 40^\circ$, the intensity loss due to cosine projection loss is $\cos 40^\circ = 0.77$, leading to a $\approx 33\%$ reduction in apparent efficiency at maximum incident angle.

D.6 Test setup for complete system

When measuring efficiency of the completed system, the camera does not have access to directly look at a surface illuminated by the system, because the surface is illuminated from the inside as shown in Figure D.11. Instead, photos are shot of the back-side of illuminated paper.

The test setup consists of shooting three photos of back-illuminated pieces of paper:

- Direct sunlight, with paper normal to incident sunlight. Gives reference solar irradiance.
- Prototype solar cooker with beam-steering lens array.
- Prototype solar cooker without beam-steering lens array.

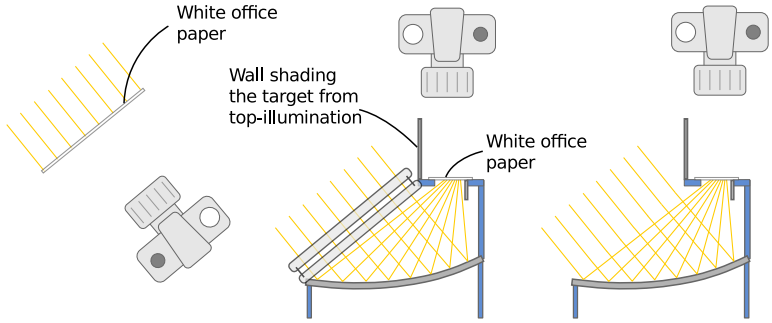

Figure D.11: Test setup for measuring performance of complete prototype system.

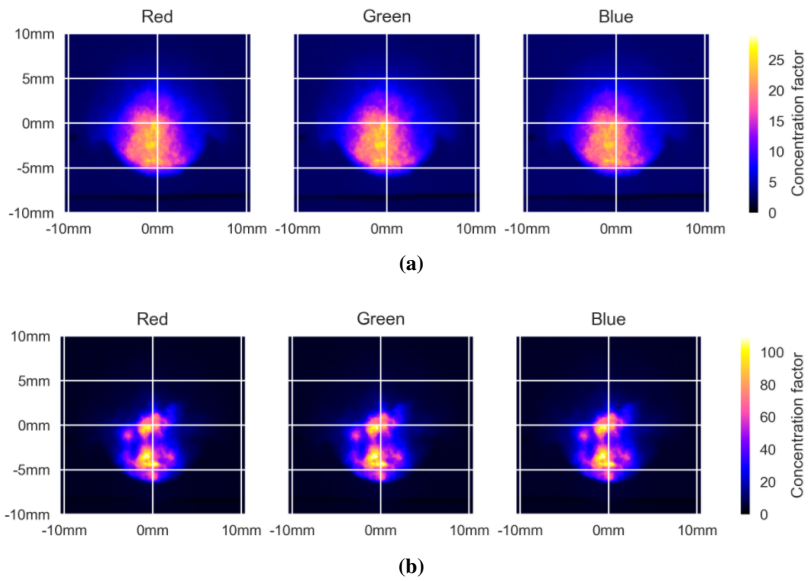

Figure D.12: Analyzed flux distribution in focal spots with (a) and without (b) beam-steering lens array. The concentration factor is fairly low even without beam-steering lens array, which is caused by a combination of poor surface quality on the parabolic reflector and a slightly unfocused system.

D.6.1 Measurement accuracy

The difference between focused and unfocused intensity is so large that the photos in this test must be shot using different exposure values. For measurements of the complete system, this the measurements can be shot by only changing ISO settings, so that it is possible to stay within the $\approx \pm 2\%$ measurement uncertainty as explained in Section D.4 on page 80. When measuring the efficiency of the bare reflector without beam-steering lens array, the focus is so intense that all camera exposure settings must be changed, giving an uncertainty of $\approx \pm 15\%$.

There are a number of other factor that add uncertainty to these measurements: It is assumed that the back-illuminated paker transmits light diffusely, so the brightness of a point on the piece of paper is proportional to the amount of sunlight striking that point from the other side. This assumption is violated by several effects, amon others nonuniform transmittance of the paper due to varying fiber density. These factors have not been quantified, but they mean that the measurements can only be approximate indications of system performance, and not be used for accurate characterization.

References

[1] Python Software Foundation. *Python programming language*. URL: `https://www.python.org/` (visited on 05/29/2017).

[2] Maik Riechert. *rawpy: Python wrapper for the LibRaw library*. URL: `https://github.com/letmaik/rawpy` (visited on 05/29/2017).

[3] Yunus Cengel and Afshin Ghajar. *Heat and Mass Transfer: Fundamentals and Applications + EES DVD for Heat and Mass Transfer*. English. 4 edition. New York: McGraw-Hill Science/Engineering/Math, Feb. 2010. ISBN: 978-0-07-736664-3.

[4] *Standard Solar Spectra — PVEducation*. URL: `http://www.pveducation.org/pvcdrom/appendices/standard-solar-spectra` (visited on 05/30/2017).

Appendix E

Risk assessment

APPENDIX E. RISK ASSESSMENT

NTNU	Kartlegging av risikofylt aktivitet	Utarbeidet av	Nummer	Dato
		HMS-avd.	HMSRV2601	22.03.2011
		Godkjent av		Erstatter
HMS		Rektor		01.12.2006

Enhet: Institutt for maskinteknikk og produksjon **Dato: 2017.01.31**

Linjeleder: Torgeir Welo

Deltakere ved kartleggingen (m/ funksjon)**:** Håkon J D Johnsen, student / Jan Torgersen, veileder
(Ansv. veileder, student, evt. medveiledere, evt. andre m. kompetanse)

Kort beskrivelse av hovedaktivitet/hovedprosess: Masteroppgave student Håkon J D Johnsen. Novel Low Cost Solar Thermal Energy Concepts for Developing Countries

Er oppgaven rent teoretisk? (JA/NEI)**:** **NEI** *«JA» betyr at veileder innestår for at oppgaven ikke inneholder noen aktiviteter som krever risikovurdering. Dersom «JA»: Beskriv kort aktiviteteten i kartleggingskjemaet under. Risikovurdering trenger ikke å fylles ut.*

Signaturer: *Ansvarlig veileder:* Jan Torgersen *Student:* Håkon J D Johnsen

ID nr.	Aktivitet/prosess	Ansvarlig	Eksisterende dokumentasjon	Eksisterende sikringstiltak	Lov, forskrift o.l.	Kommentar
1	Produksjon av prototype					
1a	Bruk av 3D printer i Troll labs	HJDJ	Maskinens brukermanual	Ukjent	Ukjent	
1b	Støping av linsesystemer	HJDJ	Produktets brukermanual og datablad	Datablad	Ukjent	
2	Testing av prototype i kunstig eller ekte sollys	HJDJ			Ukjent	

NTNU	Risikovurdering	Utarbeidet av	Nummer	Dato
		HMS-avd.	HMSRV2601	22.03.2011
		Godkjent av		Erstatter
HMS		Rektor		01.12.2006

ID nr	Aktivitet fra kartleggings-skjemaet	Mulig uønsket hendelse/ belastning	Vurdering av sannsyn-lighet (1-5)	Vurdering av konsekvens: Menneske (A-E)	Ytre miljø (A-E)	Øk/ materiell (A-E)	Om-dømme (A-E)	Risiko-Verdi (menneske)	Kommentarer/status Forslag til tiltak
1a	Bruk av 3D-printer	Brannskade	3	B	A	A	A	3B	Vær nøye med opplæring i bruk av maskin.
1a		Innhalering av plast/ printemateriale	5	A	A	A	A	5A	Bruk åndedretsvern/ vernebriller
1a		Feil bruk-> ødelagt maskineri	3	A	A	C	A	3A	Vær nøye med opplæring i bruk av maskin.
1b	Støping av linsesystemer	Eksponering på øyet	2	D	A	A	B	2D	Bruk øyevern, ha datablad tilgjengelig
1b		Eksponering hud	4	A	A	A	A	4A	Bruk hansker, ha datablad tilgjengelig
1b		Eksponering åndedrett	4	A	A	A	A	4A	Bruk åndedretsvært/ god ventilasjon. Ha datablad tilgjengelig.
1b		Søl	4	A	B	A	A	4A	Ha papir/ rengjøringsmateriell tilgjengelig. Ha datablad tilgjengelig.
1b		Brannskade	3	B	A	A	A	3B	Bruk hansker ved håndtering av varme materialer.
2	Testing av prototype i kunstig eller ekte sollys	Øyeskade-sollys	2	D	A	A	C	2D	Bruk øyevern!
2		Brannskade	3	B	A	A	A	3B	Vær forsiktig. Design prototype som begrenser fokuspunktets mulige posisjoner.

NTNU	Risikovurdering	Utarbeidet av	Nummer	Dato
		HMS-avd.	HMSRV2601	22.03.2011
		Godkjent av		Erstatter
HMS		Rektor		01.12.2006

Sannsynlighet vurderes etter følgende kriterier:

Svært liten 1	Liten 2	Middels 3	Stor 4	Svært stor 5
1 gang pr 50 år eller sjeldnere	1 gang pr 10 år eller sjeldnere	1 gang pr år eller sjeldnere	1 gang pr måned eller sjeldnere	Skjer ukentlig

Konsekvens vurderes etter følgende kriterier:

Gradering	Menneske	Ytre miljø Vann, jord og luft	Øk/materiell	Omdømme
E Svært Alvorlig	Død	Svært langvarig og ikke reversibel skade	Drifts- eller aktivitetsstans >1 år.	Troverdighet og respekt betydelig og varig svekket
D Alvorlig	Alvorlig personskade. Mulig uførhet.	Langvarig skade. Lang restitusjonstid	Driftsstans > ½ år Aktivitetsstans i opp til 1 år	Troverdighet og respekt betydelig svekket
C Moderat	Alvorlig personskade.	Mindre skade og lang restitusjonstid	Drifts- eller aktivitetsstans < 1 mnd	Troverdighet og respekt svekket
B Liten	Skade som krever medisinsk behandling	Mindre skade og kort restitusjonstid	Drifts- eller aktivitetsstans < 1uke	Negativ påvirkning på troverdighet og respekt
A Svært liten	Skade som krever førstehjelp	Ubetydelig skade og kort restitusjonstid	Drifts- eller aktivitetsstans < 1dag	Liten påvirkning på troverdighet og respekt

Risikoverdi = Sannsynlighet x Konsekvens
Beregn risikoverdi for Menneske. Enheten vurderer selv om de i tillegg vil beregne risikoverdi for Ytre miljø, Økonomi/materiell og Omdømme. I så fall beregnes disse hver for seg.

Til kolonnen "Kommentarer/status, forslag til forebyggende og korrigerende tiltak":
Tiltak kan påvirke både sannsynlighet og konsekvens. Prioriter tiltak som kan forhindre at hendelsen inntreffer, dvs. sannsynlighetsreduserende tiltak foran skjerpet beredskap, dvs. konsekvensreduserende tiltak.

NTNU	Risikomatrise	utarbeidet av	Nummer	Dato
		HMS-avd.	HMSRV2604	08.03.2010
		godkjent av		Erstatter
HMS/KS		Rektor		09.02.2010

MATRISE FOR RISIKOVURDERINGER ved NTNU

KONSEKVENS						
	Svært alvorlig	E1	E2	E3	E4	E5
	Alvorlig	D1	D2	D3	D4	D5
	Moderat	C1	C2	C3	C4	C5
	Liten	B1	B2	B3	B4	B5
	Svært liten	A1	A2	A3	A4	A5
		Svært liten	Liten	Middels	Stor	Svært stor
		SANNSYNLIGHET				

Prinsipp over akseptkriterium. Forklaring av fargene som er brukt i risikomatrisen.

Farge		Beskrivelse
Rød		Uakseptabel risiko. Tiltak skal gjennomføres for å redusere risikoen.
Gul		Vurderingsområde. Tiltak skal vurderes.
Grønn		Akseptabel risiko. Tiltak kan vurderes ut fra andre hensyn.